


Barrier-crossing times for different non-Markovian friction in well and barrier: A numerical studyFlorian N. Brüning¹, Roland R. Netz¹ and Julian Kappler^{2,*}¹*Department of Physics, Freie Universität Berlin, 14195 Berlin, Germany*²*Department of Applied Mathematics and Theoretical Physics, Centre for Mathematical Sciences, University of Cambridge, Wilberforce Road, Cambridge CB3 0WA, United Kingdom* (Received 3 May 2022; accepted 21 July 2022; published 24 October 2022)

We introduce a generalized Langevin model system for different non-Markovian effects in the well and barrier regions of a potential, and use it to numerically study the barrier-crossing time. In the appropriate limits, our model interpolates between the theoretical barrier-crossing-time predictions by Grote and Hynes (GH), as well as by Pollak *et al.*, which for a single barrier memory time can differ by several orders of magnitude. Our model furthermore allows one to test an analytic rate theory for space-inhomogeneous memory, which disagrees with our numerical results in the long well-memory regime. In this regime, we find that short barrier memory decreases the barrier-crossing time as compared to long barrier memory. This is in contrast with the short well-memory regime, where both our numerical results and the GH theory predict an acceleration of the barrier crossing time with increasing barrier memory time. Both effects, the “Markovian-barrier acceleration” and GH “non-Markovian-barrier acceleration,” can be understood from a committor analysis. Our model combines finite relaxation times of orthogonal degrees of freedom with a space-inhomogeneous coupling to such degrees and represents a step towards more realistic modeling of reaction coordinates.

DOI: [10.1103/PhysRevE.106.044133](https://doi.org/10.1103/PhysRevE.106.044133)**I. INTRODUCTION**

Many physical systems are comprised of large numbers of interacting degrees of freedom. A standard approach towards understanding dynamics in such systems is to define a low-dimensional reaction coordinate, motivated by the phenomenon to be investigated, and to construct an effective model for the dynamics of this reaction coordinate [1–10]. Hereby, the orthogonal degrees of freedom are subsumed into an effective heat bath, which interacts with the reaction coordinate [1–4]. One is then typically interested in the long-time dynamics of the reaction coordinate and in particular rare events such as barrier-crossing phenomena characterized by mean first-passage times (MFPTs), τ_{MFP} [7,11–18]. Systems where this approach has been applied are molecules in solution, which show conformational transitions, for example, protein folding [7,19–22], chemical reactions, where the reaction coordinate characterizes the transition from reactants to products [13,23–28], and vibrational spectroscopy [29,30].

If the dissipative coupling between reaction coordinate and heat bath is assumed linear, the dynamics is described by an approximate version of the generalized Langevin equation (GLE), with memory effects due to the finite relaxation time of the heat bath [2,31]. However, in many physical sys-

tems the dissipative interaction between reaction coordinate and heat bath depends nonlinearly on the current state of the reaction coordinate [3]. For example, a small molecule traversing a membrane separating two different fluids, as illustrated in Fig. 1(a), clearly interacts with different orthogonal degrees of freedom, namely, fluid or membrane molecules, depending on where it is currently located. As a second example, a reaction coordinate describing the folding of a protein is expected to experience different friction depending on whether the protein is unfolded or folded. Even for a single confined solute particle in a fluid, the nonlinear dissipative interaction of the particle and its surrounding fluid molecules leads to confinement-dependent memory effects [32]; for colloidal particles in a viscoelastic fluid, such nonlinear solute-solvent interactions have been observed experimentally [33].

The first analytical relation between the friction magnitude and the barrier-crossing time was derived by Kramers [11]. Kramers considered the memoryless, i.e., Markovian, Langevin equation with homogeneous friction magnitude. He showed that, while in the high-friction limit τ_{MFP} scales linearly with the friction, in the low-friction scenario τ_{MFP} scales linearly with the inverse of the friction magnitude. The crossover between these two asymptotic results was eventually bridged by a theory due to Melnikov and Meshkov [15] (MM), which is valid for all values of the friction magnitude.

For the scenario where there is no timescale separation between heat bath and reaction coordinate, so that non-Markovian memory effects are relevant, the first theory to describe barrier-crossing times is due to Grote and Hynes (GH) [13]. In their theory, only the local memory effects in the barrier region are taken into account, and away from the barrier region the reaction coordinate is assumed Markovian.

*Corresponding author: jkappler@posteo.de

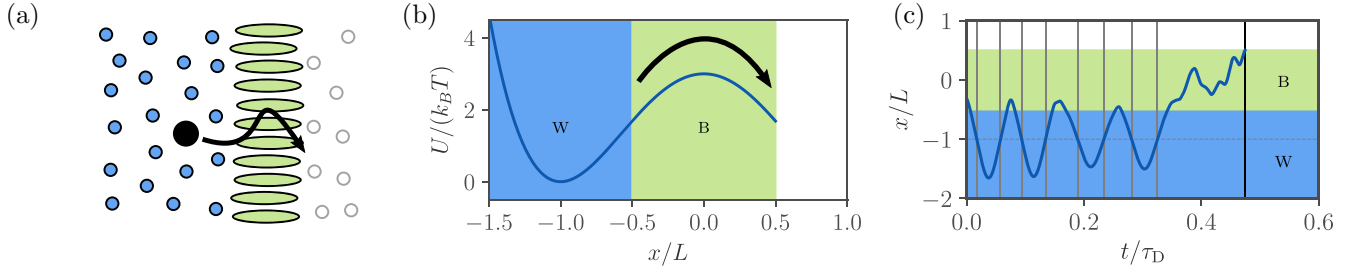


FIG. 1. (a) The dynamics of a particle diffusing through a membrane, separating different solvent species, serves as an illustrative example for space-inhomogeneous friction effects. (b) The truncated quartic potential Eq. (5) is used to model barrier-crossing dynamics. The colors indicate regions X_i with different local friction. (c) Example trajectory, simulated using single-exponentially decaying locally coupled memory-friction components, Eq. (6), with $\tau_w/\tau_D = 1$ and $\tau_b/\tau_D = 0.01$, that together form the friction kernel of Eq. (2). The coupling function $\chi_i(x)$ is given by Eq. (3) for the regions X_i , also shown in (b). The mean first-passage time (MFPT), τ_{MFP} , for barrier crossing is defined as the average of all time differences between crossings of the well bottom at $x/L = -1$ (shown as vertical gray solid lines) to the escape at the boundary at $x/L = 0.5$ (shown as a vertical black solid line).

For the case of homogenous memory effects throughout the well and barrier regions, Pollack, Grabert, and Hänggi (PGH) derived τ_{MFP} , which for long memory scales quadratically with the memory time, so that the former can exceed the latter by orders of magnitude [34]. For the special case of a single-exponential memory function, the quadratic scaling of τ_{MFP} with memory time was also derived analytically from a harmonic approximation, and a simple heuristic formula which reproduces the results of the PGH theory was proposed [35]. Importantly, for systems with long memory, the predictions of the barrier-crossing time by the PGH and GH theories differ by many orders of magnitude. Evidently it is crucial whether the coupling between reaction coordinate and heat bath is linear throughout well and barrier region (homogeneous friction) or nonlinear and thus different in well and barrier region (space-inhomogeneous friction) [35,36].

For homogeneous friction, there exist numerical studies of barrier crossing considering both single-timescale memory [7,35,37–39], as well as the implications of several memory timescales [21,40]. Models incorporating space-inhomogeneous friction have so far mostly been studied in the double limit where inertial and memory effects are negligible and can thus be modeled via an overdamped Langevin equation [41] or the equivalent Fokker-Planck equation [42,43]. However, this limit is subtle, as non-Markovian memory effects can generate spurious space-inhomogeneous friction if interpreted in terms of a Markovian model [22]. For space-inhomogeneous memory friction magnitude with a single homogeneous timescale, some works observed significant deviations of τ_{MFP} in both analytic theory and simulations when compared to the space-homogeneous case [44–46]. The implications of space-inhomogeneous memory timescales in the well and barrier regions on the global barrier-crossing dynamics have so far been addressed only by an analytical model [47–49] which bridges the GH and PGH scenarios in certain limits. However, this model has never been challenged by numerical simulations.

We here present a model system to study space-inhomogeneous friction memory times and magnitudes, which in the appropriate parameter regimes reproduces the predictions of both the PGH and GH theory. Our model is

based on the nonlinear Zwanzig model [3,48]. Importantly, while the model makes certain simplifying assumptions that are not guaranteed to hold for general systems, it allows us to study under which conditions τ_{MFP} is determined dominantly by the memory friction either in the well or in the barrier region. Specifically, we consider a reaction coordinate subject to a potential well, bounded by a moderate barrier on one side, as illustrated in Fig. 1(b). In the well and barrier regions the reaction coordinate is locally coupled to independent heat baths, each with a single finite and in general different relaxation time. This local coupling leads to space-inhomogeneous single-exponential memory in the reaction coordinate, and by independently varying the memory effects in the well and barrier region we disentangle the effects of space-inhomogeneous memory times, τ_w for the well and τ_b for the barrier, and friction magnitudes, γ_w and γ_b , on the barrier-crossing time. By comparing results of numerical simulations to the rate theories of the GH theory [13] and PGH theory [34] (for which we for simplicity use our previously derived heuristic formula [21]), with the latter evaluated using either the well or barrier friction, we are able to infer which theory describes the numerical results, and whether the barrier-crossing time depends dominantly on the well or barrier friction.

We present the results of our numerical study in two parts. First, we discuss the Markovian regime, for which memory effects in both the well and barrier regions are negligibly small, i.e., τ_b and τ_w are much smaller than the diffusive timescale $\tau_D = \gamma L^2/(k_B T)$, given by the friction constant γ , a length scale L and thermal energy $k_B T$. The dynamics in this regime are thus dependent only on inertial effects, which, strictly speaking, are Markovian only if both instantaneous position and velocity are used for defining a configuration. By labeling inertial effects as Markovian, we demarcate such inertial effects from non-Markovian effects due to coupling of the principle coordinate with hidden heat bath degrees of freedom. In our model inertial effects are characterized by the inertial timescale for the different friction magnitudes, $\tau_{m,B} = m/\gamma_B$ or $\tau_{m,W} = m/\gamma_W$. We find that whenever the well dynamics is in the high-friction regime, $m/\gamma_w \ll \tau_D$, then the barrier-crossing time is determined by the barrier top friction. If then, the barrier top is also in the high-friction

regime, $m/\gamma_B \ll \tau_D$, τ_{MFP} is described by Kramers' theory [11], evaluated using the friction magnitude at the barrier top. If, instead, the barrier dynamics is in the low-friction regime, $m/\gamma_B > \tau_D$, while γ_B and γ_W are not too different, then the MM theory [15] or PGH theory [34], evaluated using the barrier parameters, describes the numerically obtained barrier-crossing times. On the other hand, if the dynamics in the well is in the low-friction regime, $m/\gamma_W > \tau_D$, then τ_{MFP} is described by the PGH theory or MM theory, both evaluated using the well parameters, which therefore dominates the global barrier-crossing dynamics.

In the second part we discuss the non-Markovian regime, where memory effects in either well or barrier regions are relevant, i.e., either τ_B or τ_W is of at least similar order as the diffusive timescale τ_D . For simplicity we keep the friction magnitudes equal, $\gamma_B = \gamma_W$, and consider the high-friction regime by imposing $m/\gamma_B = m/\gamma_W \ll \tau_D$. Analogous to the previous case, we find that whenever the well dynamics is in the Markovian regime, $\tau_W \ll \tau_D$, then the barrier-crossing time is determined by the barrier top friction. If then again, the barrier top is also in the Markovian regime, $\tau_B \ll \tau_D$, τ_{MFP} is described by Kramers' theory [11], evaluated using the friction parameters for the barrier top. If, instead, memory effects in the barrier region are relevant, then the GH theory [13] agrees with the numerically obtained barrier-crossing times. In contrast, if the well memory is long, $\tau_W > \tau_D$, τ_{MFP} is described by the PGH theory using the well parameters. While then in general τ_{MFP} is rather independent of the barrier friction, Markovian barrier dynamics lead to a speed up of τ_{MFP} as compared to a barrier region with long memory. This speedup, which we term the ‘‘Markovian-barrier acceleration,’’ is not captured by any presently available rate theory, but can be understood from a committor analysis, analogous to the ‘‘non-Markovian-barrier acceleration’’ already predicted by the GH theory.

The remainder of this paper is organized as follows. In Sec. II we first introduce the space-inhomogeneous memory model we consider. In Sec. III we then compare numerical simulations of our model to rate-theory predictions. We first consider the short-memory limit and subsequently study how local memory effects modify τ_{MFP} . In our concluding Sec. IV we provide a table which summarizes our results.

II. MODEL

We consider a reaction coordinate x and N noninteracting heat baths with finite relaxation dynamics [3,48]; for $x \in X_i$, the reaction coordinate couples linearly to the i th heat bath. As we show in Appendix A 1, integrating out the bath degrees of freedom then leads to a GLE

$$m\ddot{x}(t) = - \int_0^t dt' \Gamma[t-t', x(t), x(t')] \dot{x}(t') - \partial_x U[x(t)] + \eta[x(t), t], \quad (1)$$

which is a generalization of the model proposed by Zwanzig [3]. $U[x(t)]$ is a potential landscape, and the space- and time-

dependent friction kernel $\Gamma[t-t', x(t), x(t')]$ is given as

$$\Gamma[t-t', x(t), x(t')] = \sum_{i=1}^N \chi_i[x(t)] \Gamma_i(t-t') \chi_i[x(t')], \quad (2)$$

where the purely time-dependent components Γ_i describe the internal relaxation dynamics of reservoir i , and the dimensionless functions χ_i , defined by

$$\chi_i(x) = \begin{cases} 1 & \text{if } x \in X_i, \\ 0 & \text{if } x \notin X_i, \end{cases} \quad (3)$$

describe the coupling of the reaction coordinate x to reservoir i . The terms in Eq. (2) have a simple intuitive interpretation: at any past time t' , the reaction coordinate x perturbs reservoir i via the coupling strength $\chi_i[x(t')]$; this perturbation relaxes in the heat bath for a duration $t-t'$ as described by $\Gamma_i(t-t')$, and finally couples back to the reaction coordinate at the time t via $\chi_i[x(t)]$.

As we show in Appendix A 2, the random force fulfills the fluctuation-dissipation relation

$$\beta \langle \eta[x(t), t] \eta[x(t'), t'] \rangle = \Gamma[t-t', x(t), x(t')], \quad (4)$$

where $\beta^{-1} = k_B T$ is the thermal energy with k_B the Boltzmann constant and T the absolute temperature.

For our numerical simulations we consider barrier crossing in the quartic potential

$$U(x) = U_0 \left[\left(\frac{x}{L} \right)^2 - 1 \right]^2, \quad (5)$$

with a length scale L and barrier height $\beta U_0 = 3$ (we show some results with varying barrier heights in Appendix C 2). To systematically study the effect of space-inhomogeneous memory on τ_{MFP} , we consider $N = 2$ independent heat baths with coupling regions in the well, $X_W/L = (-\infty, -0.5)$, and on the barrier, $X_B/L = [-0.5, 0.5)$, as illustrated in Fig. 1(b). For the resulting two memory kernels Γ_W and Γ_B , we consider single-exponential kernels,

$$\Gamma_i(t) = \frac{\gamma_i}{\tau_i} e^{-t/\tau_i}, \quad (6)$$

with friction magnitudes γ_i and relaxation timescales τ_i , where $i \in \{W, B\}$. This means that the particle interacts with two independent heat baths, each of which relaxes according to a single exponential.

As we show in Appendix A 3, Eq. (1) with local memory Eq. (2) can be cast into dimensionless form by introducing a diffusion timescale $\tau_D = \beta \gamma L^2$ with $\gamma = \sum_i \gamma_i$, and an inertial timescale $\tau_m = m/\gamma$. With the potential (5) and a given barrier height βU_0 , the system is then specified by four dimensionless parameters which we choose to be the dimensionless inertial timescale τ_m/τ_D , the dimensionless local memory times τ_i/τ_D , $i \in \{W, B\}$, and one of the two relative friction magnitudes γ_i/γ , $i \in \{W, B\}$. To transform dimensionless results to physical dimensions, the temperature T , the length scale L , and the sum γ of the local friction magnitudes additionally need to be specified. To simulate the dimensionless formulation of Eqs. (1), (2), and (4), we use a Markovian embedding whereby we explicitly simulate the dynamics in the reservoirs, as detailed in Appendix A 3.

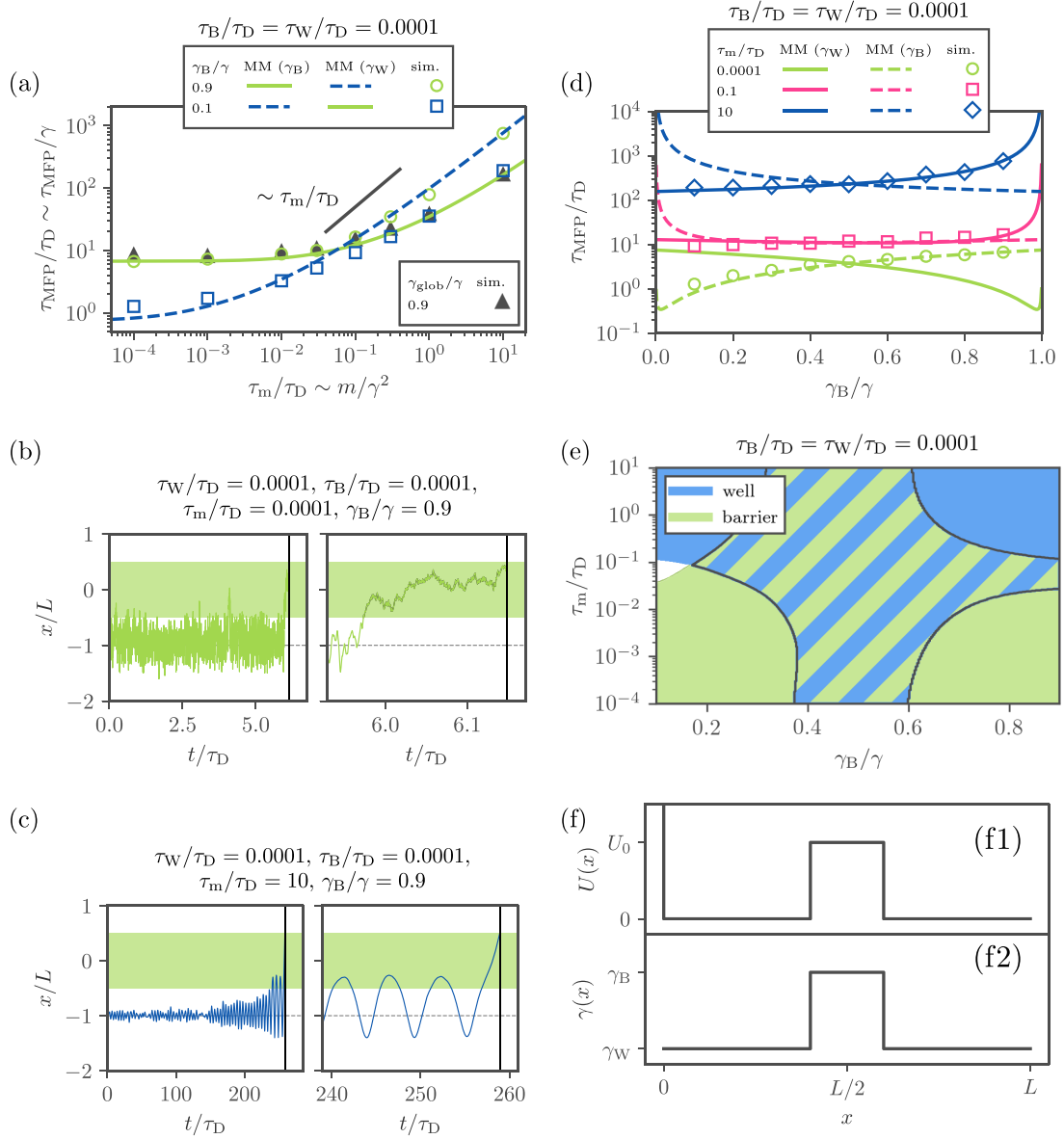


FIG. 2. MFPT, τ_{MFP}/τ_D , for different barrier memory friction, $\Gamma_B(t) = \gamma_B e^{-t/\tau_B}/\tau_B$ and well memory friction, $\Gamma_W(t) = \gamma_W e^{-t/\tau_W}/\tau_W$, obtained from numerical simulations (data points) and compared with analytical predictions given by Mel'nikov and Meshkov [15] (MM, solid and broken lines). The data are shown for various inertial timescales τ_m/τ_D and equal memory times in the Markovian limit, $\tau_B/\tau_D = \tau_W/\tau_D = 10^{-4}$. (a) τ_{MFP} plotted over the inertial timescale τ_m/τ_D for different ratios of the barrier to total friction magnitude γ_B/γ . The predictions by MM are shown for the effective barrier-friction parameters given by γ_B and for the effective well-friction parameters given by γ_W . The black triangles denote simulations with space-homogeneous friction. (b, c) Example trajectories from simulations. (d) τ_{MFP} plotted over γ_B/γ for various τ_m/τ_D . The predictions by MM are shown for the effective barrier-friction parameters as broken lines and for the effective well-friction parameters as solid lines. (e) Contour plot of agreement of the simulation results with the theoretical predictions. The color denotes whether the simulated $\tau_{\text{MFP}} \in [2/3 \tau_{\text{theo}}, 3/2 \tau_{\text{theo}}]$, where τ_{theo} is calculated using MM theory and either the effective well- or barrier-friction parameters. The hatching indicates that both theoretical predictions agree with the simulated data. White denotes that neither prediction agrees within the tolerance. (f) Model potential (f1) and friction profile (f2) used to study the effect of the barrier friction on τ_{MFP} in the high-friction Markovian regime. For this model τ_{MFP} is exactly predicted by Eq. (8).

In analogy to previous works, we define various limits by comparison of respective timescales with the diffusive timescale τ_D . For example the Markovian limit where memory effects are negligible is obtained for $\tau_i < \tau_D$, and the high-friction limit where inertial effects are negligible is obtained for $\tau_m < \tau_D$ [21,35,40]. However, since the local friction in region i , γ_i , is only part of the total friction γ , which is used to

define τ_D , a condition $\tau_i \ll \tau_D$ does not automatically ensure the expected limit in region i . Rather, a condition involving the local diffusive timescale, $\tau_{D,i} \equiv \beta L^2 \gamma_i$, needs to be used, namely, $\tau_i/\tau_{D,i} \equiv \tau_i/\tau_D(\gamma/\gamma_i) \ll 1$. Similarly, inertial effects are locally relevant for $\tau_{m,i}/\tau_{D,i} \equiv \tau_m/\tau_D(\gamma/\gamma_i)^2 \gtrsim 1$, where $\tau_{m,i} \equiv m/\gamma_i$. While the distinction between $\tau_{m,i}$, $\tau_{D,i}$ and τ_m , τ_D is important if γ_i is significantly smaller than γ , for most

of the parameter combinations we consider in the main text, all γ_i are of similar order as their sum γ .

Since we are interested in evaluating the barrier-crossing time starting from the well region X_W , we restart the simulation once the particle crosses the right boundary at $x/L = 0.5$, which we consider a successful escape. At each restart, we draw the initial position from an approximate Boltzmann distribution around the well minimum, i.e., we draw a Gaussian random variable $x(0)$ with $\langle x(0)/L \rangle = -1$ and $\langle [x(0)/L + 1]^2 \rangle = k_B T / [L^2 U''(-L)] = k_B T / (8U_0)$. Similarly, we draw the initial velocity $\dot{x}(0)$ from its equilibrium distribution, i.e., a Gaussian random variable with $\langle \dot{x}(0) \rangle = 0$ and $\langle \dot{x}^2(0) \rangle = k_B T / m$. The initial conditions for the heat bath variables we subsequently draw from their respective Boltzmann distributions, as detailed in Appendix A 2.

In Fig. 1(c) we show an example trajectory, simulated using long memory in the well and short memory on the barrier, for which different dynamics in the different regions are clearly observed: While in the well region the trajectory oscillates weakly-damped around the potential minimum, on the barrier the trajectory is more akin to overdamped diffusive dynamics. Figure 1(c) furthermore illustrates how we compute τ_{MFP} from observed time differences between crossings of the well minimum and the escape at $x/L = 0.5$. That this is a reliable method for calculating τ_{MFP} has been shown before [35].

In the main text, we compare our numerical results to the GH [13], MM [15], and PGH theory [34], where instead of the latter we use a heuristic formula [35] in practice. The GH theory accounts only for barrier memory friction, which is why we always evaluate it using the barrier memory kernel; the theory assumes fast equilibration within the well, and does not depend on the well friction explicitly. Both the Markovian MM and non-Markovian PGH theory assume homogeneous friction. We therefore evaluate these theories using either the local parameters γ_i , τ_i of the well or barrier region. This allows us to infer not only which rate theory describes the barrier-crossing dynamics in which regime, but also which region (well or barrier) dominantly determines the global τ_{MFP} . In Appendix B we summarize the equations used to calculate predictions for all rate theories considered in the main text. In the main text, we do not compare our numerical simulations to the analytical rate theory for space-inhomogeneous memory friction due to Krishnan *et al.* [48]. The reason for this is twofold: First, by comparing to the widely used GH and PGH theories, we are able to assess which local dynamics dominate the global τ_{MFP} . Second, as we show in Appendix C 4, the theoretical predictions by Krishnan *et al.* [48] do not capture the ‘‘Markovian-barrier acceleration’’ regime, which we prominently discuss below and which we quantify using the PGH predictions.

III. RESULTS

In order to decouple Markovian inertial effects and non-Markovian memory effects we analyze both scenarios independently. For this we first consider the Markovian limit, $\tau_B/\tau_D, \tau_W/\tau_D \ll 1$, and vary τ_m/τ_D , and second the high-friction limit, $\tau_m/\tau_D \ll 1$, with varying τ_B/τ_D and τ_W/τ_D .

A. Markovian friction dynamics

We now consider the Markovian limit for both well and barrier. In Fig. 2(a) we show the rescaled τ_{MFP}/τ_D as a function of the rescaled inertial time τ_m/τ_D . For reference, we include numerical results from a GLE with a homogeneous single-exponential memory kernel with memory time $\tau_{\text{glob}}/\tau_D = 10^{-4}$ and a single friction magnitude $\gamma_{\text{glob}} = 0.9 \gamma$ (chosen as to coincide with the light green solid line, as explained further below) [35]; the resulting τ_{MFP} are shown in Fig. 2(a) as black triangles, and clearly show the Kramers turnover between high-friction dynamics for $\tau_m/\tau_D \ll 1$, where τ_{MFP} scales as $\sim \gamma$, and low-friction dynamics for $\tau_m/\tau_D \gg 1$, where τ_{MFP} scales as $\sim m/\gamma$ [11, 15, 35].

Figure 2(a) furthermore shows numerical results for the space-inhomogeneous memory model Eqs. (1) and (2) for $\tau_B/\tau_D = \tau_W/\tau_D = 10^{-4}$ and the two values $\gamma_B/\gamma = 0.1, 0.9$. For $\gamma_B/\gamma = 0.1$ we have $\gamma_W/\gamma = 0.9$, so that the friction in the well is almost one order of magnitude larger as compared to the friction in the barrier region. Conversely, for $\gamma_B/\gamma = 0.9$ the friction in the well, $\gamma_W/\gamma = 0.1$, is almost one order of magnitude smaller as compared to the friction in the barrier region. While in the high-friction regime $\tau_m/\tau_D \ll 1$, the results for $\gamma_B/\gamma = 0.9$ (light green circles; barrier friction much larger than well friction) agree well with the global memory friction data (black triangles), in the low-friction regime $\tau_m/\tau_D \gg 1$, it is τ_{MFP} for $\gamma_B/\gamma = 0.1$ (dark blue squares; well friction much larger than barrier friction) that is comparable to the global memory friction result. This indicates that for high friction, τ_{MFP} is dominated by the barrier friction, whereas for low friction τ_{MFP} is dominated by the well friction.

The crossover between barrier-dominated τ_{MFP} to well-dominated τ_{MFP} observed in Fig. 2(a) is further confirmed by comparing the numerical data to predictions of the MM theory for Markovian barrier crossing, which is based on homogeneous friction. In Fig. 2(a) we show the predictions of MM theory, evaluated using either the well friction γ_W or the barrier friction γ_B . Note that because of the symmetry in the used parameters, the light green solid line represents both the MM prediction for $\gamma_B/\gamma = 0.9$, and evaluation using the barrier friction, as well as the MM prediction for $\gamma_B/\gamma = 0.1$, and evaluation using the well friction. On the other hand, the dark blue broken line represents the opposite parameter choice in both scenarios. We observe that, while in the high-friction limit $\tau_m/\tau_D \ll 1$, the simulated τ_{MFP} agree with the MM predictions evaluated at the barrier region, for low friction $\tau_m/\tau_D \gg 1$ the numerical data are described by the MM theory evaluated at the well.

That for the Markovian high-friction scenario, τ_{MFP} is dominated by the barrier friction, follows from a simple analytical model. In the high-friction Markovian limit τ_{MFP} to start at x_0 and reach x_f in a potential $U(x)$ and for space-inhomogeneous friction $\gamma(x)$ is derived exactly from the Fokker-Planck equation as [43]

$$\tau_{\text{MFP}}(x_0, x_f) = \beta \int_{x_0}^{x_f} dx \gamma(x) e^{\beta U(x)} \int_{x_L}^x dx' e^{-\beta U(x')}, \quad (7)$$

where $x_L < x_0$ is a lower reflecting boundary. To study the effect of barrier friction on τ_{MFP} , we consider the model illustrated in Fig. 2(f): a simplified flat potential $U(x)$, which

features a reflecting boundary at $x = 0$ and a step barrier of height U_0 , width B and friction γ_B located at position $x = L/2$. Outside of the potential barrier, the friction is γ_W . Considering $x_0 = x_L = 0$ and $x_f = L$, τ_{MFP} is calculated from Eq. (7) to be

$$\tau_{\text{MFP}}^{0 \rightarrow L} = \beta \frac{L^2}{2} \gamma_W + \beta \frac{LB}{2} (\gamma_B - \gamma_W) + \beta \frac{B(L-B)}{2} (1 - e^{-\beta U_0}) (\gamma_B e^{\beta U_0} - \gamma_W). \quad (8)$$

In the high-barrier limit, where $\beta U_0 \gg 1$, Eq. (8) is dominated by an expression which contains only the barrier friction γ_B :

$$\tau_{\text{MFP}}^{0 \rightarrow L} \approx \beta \gamma_B \frac{B(L-B)e^{\beta U_0}}{2}. \quad (9)$$

This result explains why the τ_{MFP} in the high-friction scenario is determined by the barrier friction.

Example trajectories, comparing the cases of Markovian high-friction dynamics ($\tau_m/\tau_D = 10^{-4}$), where τ_{MFP} is determined by the barrier friction, and Markovian low-friction dynamics ($\tau_m/\tau_D = 10$), where τ_{MFP} is determined by the well friction, are shown in Figs. 2(b) and 2(c). While the trajectory in Fig. 2(b) generally exhibits dynamics reminiscent of Markovian high-friction Langevin dynamics around the well and also in the barrier region, differences in the lengths of persistent motion due to the vastly different local friction magnitudes are clearly visible. The trajectory in Fig. 2(c) shows oscillations within the wells and long residence times, which are typical of inertia-dominated stochastic dynamics [35].

Figure 2(d) shows the numerical τ_{MFP} , plotted as a function of the relative barrier friction γ_B/γ for various values of the rescaled inertial time τ_m/τ_D . Again, while for high friction, $\tau_m/\tau_D = 10^{-4}$, the simulated data agree with the MM theory evaluated using the barrier friction (light green broken line), for large $\tau_m/\tau_D = 10$ the numerical results agree with the predictions using the well friction (dark blue solid line). We observe that for the parameters considered, the rescaled τ_{MFP}/τ_D always increases monotonously with γ_B/γ , indicating that increasing barrier friction while decreasing well friction slows down barrier-crossing. The analytical MM theory shows nonmonotonicities for the case of high total friction, $\tau_m/\tau_D = 10^{-4}$, but very unequal friction magnitudes in well and barrier regions, $\gamma_i/\gamma \ll 1$, i.e., to the far right and left of Fig. 2(d). This is discussed in detail in Appendix C 1.

Figure 2(e) illustrates for which parameters the simulated τ_{MFP} is described by the theoretical predictions of MM theory, evaluated for either the well- or barrier-friction parameters. The figure again clearly shows that for high-friction dynamics, $\tau_m/\tau_D \ll 0.1$, τ_{MFP} is determined by the barrier friction, whereas for low-friction dynamics, the well friction determines τ_{MFP} . The hatched area shows the overlap where both predictions calculated using well or barrier friction agree with the simulated τ_{MFP} . Obviously, in the crossover between barrier- and well-dominated friction, where $\gamma_B \approx \gamma_W$, the rate theories produce similar results when evaluated using barrier or well friction; see also Fig. 2(d). This is because for $\gamma_B/\gamma \approx 0.5$, we have $\gamma_W/\gamma = (\gamma - \gamma_B)/\gamma \approx 0.5$, so that the effective friction magnitudes in well and barrier region, and hence the predictions of MM theory, which depend on the effective local friction, are similar.

To summarize Figs. 2(a)–2(e), in the Markovian (short memory) limit, the rescaled τ_{MFP} is for high-friction dynamics determined by the barrier friction, whereas for low-friction dynamics it is determined by the well friction. The former effect is illustrated by the analytical result Eq. (9), while the latter is intuitively understood from the concept of energy diffusion. For low-friction dynamics the energy exchange between the reaction coordinate and the heat bath is weak and therefore the energy to cross the potential barrier is only slowly built up in the well region. This process is dominated by the well dynamics and leads to a slow-down of the global barrier-crossing times. Since slow energy diffusion is also apparent for long memory times, a similar effect is observed in the discussion of the non-Markovian dynamics in the following.

B. Non-Markovian friction dynamics

In Fig. 3 we investigate the memory-time dependence of τ_{MFP} . For this, we consider a constant inertial timescale in the high-friction limit, $\tau_m/\tau_D = 10^{-4}$, and identical friction magnitudes for the two reservoirs, $\gamma_W/\gamma = \gamma_B/\gamma = 0.5$, while varying the well- and barrier-friction timescales, τ_W/τ_D and τ_B/τ_D . We compare our numerical results to analytical predictions based on both the GH theory [13], which we evaluate using the barrier-friction parameters τ_B , γ_B and which is hence independent of the well parameters, and PGH theory [34] (for which we in practice use a heuristic formula [21]), which we evaluate for both the well parameters τ_W , γ_W or the barrier parameters τ_B , γ_B .

In Fig. 3(a) we show the rescaled τ_{MFP} as a function of the barrier memory time τ_B/τ_D for various fixed well memory times τ_W/τ_D . For short barrier memory, $\tau_B/\tau_D \ll 0.1$, the dynamics on the barrier top is Markovian and the numerical τ_{MFP} are independent of τ_B/τ_D . If additionally also the memory in the well is short, $\tau_W/\tau_D \ll 0.1$, we are in the Markovian high-friction limit. While, as we have already discussed in the context of Fig. 2(a), in this limit the barrier-crossing time is determined by the barrier friction, the PGH theory evaluated with well friction (black solid line) agrees with the PGH theory evaluated with barrier friction (colored solid lines) and GH theory (black broken line; always evaluated at barrier friction); this is because we have equal friction magnitudes in well and barrier. While in the double limit of high friction and short well memory $\tau_W/\tau_D \leq 0.01$, all theories describe the numerical data (shown as circle and square markers) as long as $\tau_B/\tau_D \ll 0.01$, for $\tau_B/\tau_D \gtrsim 0.01$, both the GH theory and numerical results display an acceleration (as compared to the Markovian limit $\tau_B/\tau_D \rightarrow 0$); we refer to this as GH “non-Markovian-barrier acceleration.” That the GH theory describes this acceleration regime is expected because it was derived assuming fast equilibration within each well, which is in line with the high-friction Markovian dynamics inside the well for $\tau_m/\tau_D = 10^{-4}$, $\tau_W/\tau_D \leq 0.01$. We note that in the limit of $\tau_B/\tau_D \rightarrow \infty$, the GH theory agrees with the predictions of transition state theory [13]. For high-friction dynamics with short well memory, τ_{MFP} is thus determined by the barrier friction and described by the GH theory.

On the other hand, for long memory in the well, $\tau_W/\tau_D \geq 1$, the numerical τ_{MFP} (dark purple diamonds and dark blue

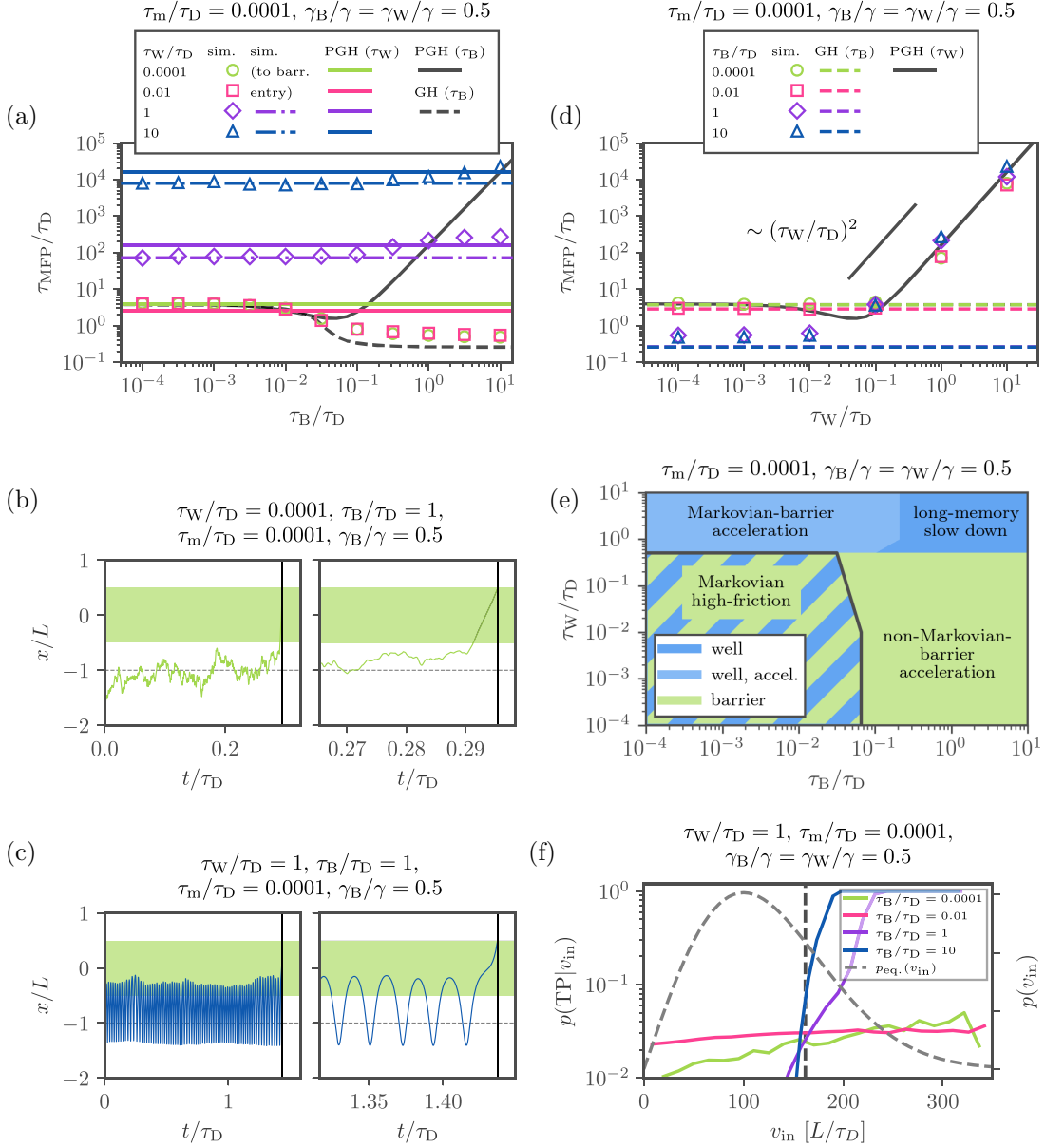


FIG. 3. MFPT, τ_{MFP}/τ_D , for different barrier memory friction, $\Gamma_B(t) = \gamma_B/\tau_B e^{-t/\tau_B}$ and well memory friction, $\Gamma_W(t) = \gamma_W/\tau_W e^{-t/\tau_W}$, from numerical simulations (data points) compared with analytical predictions given by Grote and Hynes [13] (GH, broken lines) and Pollak *et al.* [34] (PGH, solid lines, evaluated using the heuristic formula [21]). The data are shown for various barrier-friction τ_B/τ_D and well-friction times τ_W/τ_D , constant inertial timescale in the high-friction limit $\tau_m/\tau_D = 10^{-4}$, and equal friction magnitudes $\gamma_B/\gamma = \gamma_W/\gamma = 0.5$. (a) τ_{MFP} plotted over the barrier-friction time τ_B/τ_D (data points). The theories are shown for the respective barrier-friction time in black and in the case of the PGH theory for the well-friction time as colored lines. Simulated τ_{MFP} to reach the barrier entry at $x/L = -1/2$ are shown as colored dash-dotted lines. (b, c) Example trajectories from simulations for the barrier-dominated and GH-predicted limit (b) and the well-dominated PGH-predicted limit (c). (d) τ_{MFP} plotted over the well-friction time τ_W/τ_D (data points). The theories are shown for the respective well-friction time in black and in the case of the GH theory for the barrier-friction time as colored broken lines. (e) Contour plot of agreement of the simulation results with the theoretical predictions. The color denotes whether the simulated $\tau_{\text{MFP}} \in [1/3 \tau_{\text{theo}}, 3 \tau_{\text{theo}}]$, where τ_{theo} is calculated using either the GH theory with the barrier-friction parameters or the PGH theory with the well-friction parameters. The hatching indicates that both theoretical predictions agree with the simulated data. The light blue area denotes the “Markovian-barrier acceleration” of the PGH prediction for which we define $\tau_{\text{theo,MBA}} = 0.2 \tau_{\text{theo,PGH}}$. (f) Committor $p(\text{TP}|v_{\text{in}})$ for transition paths crossing the barrier region plotted over the initial velocity v_{in} upon entering the barrier region for various barrier-friction times τ_B/τ_D and constant well-friction time $\tau_W/\tau_D = 1$ and inertial time $\tau_m/\tau_D = 10^{-4}$. The velocity related to the difference in potential energy relative to the barrier top is plotted as a vertical black broken line. The flux-weighted equilibrium velocity distribution $p_{\text{eq}}(v_{\text{in}})$ is plotted as a gray broken line on a linear scale.

triangles) are comparable to the predictions of the PGH theory evaluated with the well parameters, and even for a Markovian barrier, $\tau_B/\tau_D \ll 1$, disagree considerably with the GH theory (which indicates a breakdown of the assumption of fast equilibration within the well inherent to the GH theory). In contrast to the Markovian-well scenario, for long well memory τ_{MFP} is thus determined by the well dynamics. Interestingly, in the long-well-memory regime, $\tau_W/\tau_D \geq 1$, the observed τ_{MFP} show a slight acceleration for small barrier-memory times $\tau_B/\tau_D \lesssim 0.1$, as compared to the predictions by the PGH theory and the numerical results for $\tau_B/\tau_D \gg 0.1$. We here refer to this acceleration due to short barrier memory as “Markovian-barrier acceleration,” which notably behaves opposite as a function of τ_B as compared to GH “non-Markovian-barrier acceleration,” as we discuss further below.

Figures 3(b) and 3(c) show example trajectories where τ_{MFP} is determined by barrier or well friction. For the trajectory shown in Fig. 3(b) τ_{MFP} is determined by the barrier friction, and we observe high-friction Markovian dynamics within the well and a direct transition path upon entering the barrier region. The trajectory with well-friction-determined τ_{MFP} , Fig. 3(c), on the other hand shows a long residence time in the well, and multiple attempts entering the barrier region before crossing over the barrier top, that are associated with energy-diffusion, i.e., memory- or inertia-dominated trajectories [35].

In Fig. 3(d) we show the numerical τ_{MFP} as function of the well memory time τ_W/τ_D , for several constant values of the barrier memory time τ_B/τ_D . We again compare to theoretical predictions based on the PGH and GH theories. Similar to Fig. 3(a) we see that for short well memory, $\tau_W/\tau_D \ll 0.1$, τ_{MFP} becomes independent of the well memory time so that the dynamics is governed by the barrier. If additionally the barrier memory time is short, $\tau_B/\tau_D \ll 0.1$, then τ_{MFP} is described by both the PGH (evaluated in the well) and GH theory. Increasing the barrier memory time τ_B/τ_D then leads to an acceleration of barrier crossing as we discussed in Fig. 3(a), and as described by the GH theory [leftmost data points in Fig. 3(d)]. For any value of the barrier memory τ_B/τ_D , we observe that as the well memory is increased, for $\tau_W/\tau_D \gtrsim 1$ an asymptotic long-memory regime with $\tau_{\text{MFP}} \sim \tau_W^2$ is reached [35], which is well described by the PGH theory evaluated at the well. Increasing the well memory time τ_W/τ_D thus has both a qualitatively and quantitatively very different effect from increasing the barrier memory time τ_B/τ_D where, as demonstrated in Fig. 3(a), τ_{MFP} slightly increases/decreases (depending on τ_W/τ_D) and then becomes independent of τ_B/τ_D .

Figure 3(e) summarizes the agreement of the simulated high-friction τ_{MFP} with the PGH theory, evaluated on well parameters, and the GH theory, which is always evaluated using the barrier parameters. We see that once the well memory becomes relevant, i.e., for $\tau_W/\tau_D \gtrsim 0.1$, τ_{MFP} is approximately described by PGH theory evaluated at the well. The “Markovian-barrier acceleration” regime appears if memory in the well is relevant, but in the barrier region the memory time is short, i.e., for $\tau_B/\tau_D \ll 1$, $\tau_W/\tau_D \gtrsim 1$, and is shown as light blue. If well memory effects are negligible, i.e., for $\tau_W/\tau_D \ll 0.1$, but memory effects are relevant in the barrier

region, $\tau_B/\tau_D \gg 0.1$, then GH theory describes the numerical results. If memory effects are negligible for both well and barrier region, $\tau_W/\tau_D \ll 1$ and $\tau_B/\tau_D \ll 0.1$, then we are in the Markovian limit, where the barrier friction γ_B determines τ_{MFP} . That in this regime both GH theory (evaluated at the barrier region) and PGH theory (evaluated at the well region) describe the numerical τ_{MFP} , as indicated by the hatching, can be rationalized by the fact that we use the same friction magnitude for well and barrier, $\gamma_B = \gamma_W$.

C. Markovian-barrier acceleration

In order to gain intuition about the “Markovian-barrier acceleration” regime, i.e., the slight barrier-crossing speed-up observed for $\tau_W/\tau_D \gtrsim 1$, $\tau_B/\tau_D \ll 1$ in Figs. 3(a) and 3(d), we perform a committor analysis, the results of which are shown in Fig. 3(f). The committor shown in the figure is defined as the probability to be on a transition path through the barrier region, and plotted as a function of the initial velocity with which the particle enters the barrier region, v_{in} . For comparison, the flux-weighted equilibrium velocity probability density, $p_{\text{eq}}(v) \propto v \exp[-mv^2/(2k_B T)]$ [50,51], is given as a gray broken line. Furthermore, we show as a vertical black broken line the threshold velocity v_t with which an undamped particle entering the barrier region crosses over the barrier top, so that $mv_t^2/2 = U_0 - U(x = -L/2) = 7U_0/16$, and hence $v_t = \sqrt{7U_0/(8m)}$.

For short memory in the barrier region, $\tau_B/\tau_D \ll 1$, the committor is relatively small and only very slightly increases with larger initial velocities (the light green and light red solid lines), indicating that the kinetic energy is quickly dissipated in the barrier region and the probability to perform a transition is approximately independent of the velocity with which the particle enters the barrier region. For long barrier memory $\tau_B/\tau_D \geq 1$, the committor remains almost zero for velocities $v_{\text{in}} \lesssim v_t$, indicating that many trajectories that enter the barrier region will simply roll back into the well region. They initially do not have enough kinetic energy to cross the barrier top and the energy exchange with the barrier heat bath is not fast enough to gain the missing energy. At v_t , the committor starts to increase sharply and saturates at a value of 1, which means that virtually every trajectory that enters the barrier region with at least this kinetic energy performs a transition through the barrier region. This is consistent with a weak energy exchange of heat bath and reaction coordinate in the barrier region, where a trajectory traverses the barrier top only if initially it has enough kinetic energy to reach there.

The physical picture for the “Markovian-barrier acceleration” regime is hence that for short barrier memory time the energy exchange between reaction coordinate and barrier heat bath is fast; this means that for high-friction Markovian barrier dynamics, a large fraction of particles entering the barrier region (without enough energy to cross the barrier top) is able to obtain the missing energy from the barrier heat bath, which leads to a decrease in τ_{MFP} with decreasing barrier memory time. Interestingly, as can be seen in Fig. 3(a), this effect changes τ_{MFP} in the opposite way as the “non-Markovian-barrier acceleration” predicted by the GH theory, and reproduced by our numerical model in the limit of high-friction Markovian dynamics in the well.

Nevertheless, the mechanisms behind both regimes are similar and can each be understood from the committor analysis shown in Fig. 3(f). “Non-Markovian-barrier acceleration” profits from the fact that in the case of long barrier memory fast initial velocities, i.e., $v_{in} \gtrsim v_t$ [to the right of the vertical black broken line in Fig. 3(f)], always lead to a direct transition. In case of short well memory, the initial velocities v_{in} of subsequent barrier crossing attempts are only weakly correlated, allowing for the assumption made by the GH theory that the equilibrium velocity distribution is sampled equally at any attempt. Consequently the high-velocity tail of the equilibrium distribution of v_{in} is visited more frequently over time compared to the long well memory case, where the initial velocity changes rather slowly for consecutive attempts, due to the weak coupling to the well heat bath. On the other hand, in the limit of long well memory the “Markovian-barrier acceleration” profits from the fact, that in the case of slow initial velocities, i.e., to the left of the vertical black broken line, and short barrier memory, there is still a small chance that a transition over the barrier occurs. This leads to a slightly faster τ_{MFP} when compared to the case that all the energy to reach the barrier top needs to be accumulated from the well heat bath.

This analysis furthermore suggests a simple way to quantify the “Markovian-barrier acceleration”: τ_{MFP} over the barrier is mainly determined by τ_{MFP} to reach the barrier region for the first time. Subsequently, a successful transition of the barrier region happens relatively quickly. On the contrary, for long barrier memory τ_{MFP} over the barrier is determined by the time to reach the barrier top. In Fig. 3(a) we therefore also compare τ_{MFP} to reach the barrier entry at $x/L = -0.5$ (dark purple and dark blue dash-dotted lines) and τ_{MFP} over the barrier to reach at $x/L = 0.5$ (the data coincide with the dark purple and dark blue solid lines), both evaluated from simulations with a global memory friction assuming the well friction parameters. As expected, the former coincide with the data of the “Markovian-barrier acceleration” regime correctly, while the later coincide with the data in the case of long barrier memory.

A comparison of all presented simulation data with the global analytical rate theory for local memory effects by Krishnan *et al.* [48] is shown in Appendix C4. Their theory performs well in some regimes of the parameter space, correctly interpolates between predictions by GH and PGH and therefore intrinsically determines whether the dynamics are well or barrier dominated. However, in certain parameter regimes, including the “Markovian-barrier acceleration” regime, major deviations from the numerical results are observed. This is due to instabilities of the perturbation theory inherent to the analytical approach, in fact, the authors themselves state that predictions in this parameter regime should be validated by simulations, as we have done here.

IV. CONCLUSIONS

We study a model for barrier crossing with different well and barrier memory friction times and magnitudes. By comparing extensive numerical simulations of this model to the GH theory (which takes into account memory friction in the barrier region) and the PGH theory (which does not take into

TABLE I. Summary of the regimes observed when varying single-exponential barrier and well memory friction, and the respective applicable rate theories with the dominant preexponential scaling factors. The GH reactive frequency λ is defined in Appendix B1. The table is approximately valid while the barrier and well friction magnitudes remain within one order of magnitude. Some effects for very different friction magnitudes in well and barrier are discussed in Appendix C1.

		Well		
		Markovian high friction	Markovian low friction	Long memory
Barrier	Markovian high friction	Barrier dominated Kramers, GH, PGH MM $\tau_{MFP} \sim \gamma_B$	Well dominated	Well dominated PGH (Markovian-barrier acceleration) $\tau_{MFP} \sim \tau_W^2/\gamma_W$
	Markovian low friction	Barrier dominated PGH MM $\tau_{MFP} \sim m/\gamma_B$	PGH MM $\tau_{MFP} \sim m/\gamma_W$	Well dominated PGH $\tau_{MFP} \sim \tau_W^2/\gamma_W$
	Long memory	Barrier dominated GH (non-Markovian-barrier acceleration) $\tau_{MFP} \sim \lambda^{-1}(\gamma_B, \tau_B)$		

account space-inhomogeneous memory), we identify in which region of the model parameter space the barrier-crossing time, in terms of the mean first-passage time, τ_{MFP} , is determined by the well memory or the barrier memory, respectively.

The memory friction around the barrier top determines τ_{MFP} only if the dynamics in the well is in the Markovian high-friction regime. In this case τ_{MFP} is described by GH theory if non-Markovian effects on the barrier are present, and instead by MM theory if Markovian low-friction effects dominate the barrier dynamics while the friction magnitudes in well and barrier are comparable.

If the dynamics in the well is in the so-called energy-diffusion regime, i.e., either dominated by inertia effects, $\tau_{m,W}/\tau_{D,W} \gtrsim 1$, or because of long memory in the well, $\tau_W/\tau_{D,W} \gtrsim 1$, then the rate-limiting step is obtaining enough energy from the well heat bath to make a barrier-crossing attempt. In this scenario, τ_{MFP} is described by the PGH theory evaluated for the well parameters. In this regime, high friction on the barrier top slightly diminishes τ_{MFP} ; this “Markovian-barrier acceleration” is due to the strong interaction between reaction coordinate and heat bath in the barrier region, which enables particles that enter the barrier region without enough energy for a barrier crossing to gain the missing energy in the barrier region and make it over the top. Interestingly, the same mechanism leads to a slow-down in the case of a Markovian well, where the “non-Markovian-barrier acceleration” correctly predicted by the GH theory happens in the limit of long barrier memory, not short barrier memory. This contrast highlights the complex interplay between barrier friction and well friction. The different regimes, and which theory needs to be evaluated where in order to describe the corresponding τ_{MFP} , are summarized in Table I. The table

allows one to quickly infer which aspect of the dynamics of a reaction coordinate determines the timescales of rare events, and will help researchers identify the appropriate rate theory for a given system.

While theoretical works often incorporate only either space-inhomogeneous friction magnitudes or homogeneous time-dependent memory friction [7–10,21,34,35,40–43], reaction coordinates in physical systems with nonlinear interactions may in general exhibit both effects simultaneously. Our model system therefore represents a step towards more realistic coarse-grained descriptions of reaction coordinates. To parametrize a GLE with both space-inhomogeneous memory friction time and magnitude, such as the one presented in this work, from time series data, an extension of methods established for homogeneous memory can be considered [7,52,53]. Furthermore, there are several relevant extensions of our model system. First, an interaction between the different coupling heat baths could be included, as in a physical system the orthogonal degrees of freedom are in general not isolated from each other. Second, it will be interesting to consider the nonequilibrium scenario where the interaction between reaction coordinate and orthogonal degrees of freedom does not originate from an interaction potential; this scenario has been studied before for homogeneous friction [54].

Quantum effects are not incorporated in the present model, but quantum projection methods have previously been discussed [55,56]. Within the Born-Oppenheimer approximation classical barrier crossing dynamics would essentially be modified by two effects: reduction of the effective barrier height due to zero-point motion and competition of the classical barrier-crossing rate with the tunneling rate [14,16]. Beyond the Born-Oppenheimer approximation, nonadiabatic effects such as electronic transitions between different energy surfaces would require multistate modeling [57].

ACKNOWLEDGMENTS

We gratefully acknowledge support by the Deutsche Forschungsgemeinschaft (DFG) grant SFB 1078, by the European Research Council under the Horizon 2020 Programme, ERC Grants Agreement No. 740269 and No. 835117, by the Royal Society through grant RP1700, and computing time on the HPC clusters at the Physics Department and at ZEDAT, FU Berlin.

F.N.B., R.R.N., and J.K. conceived the theory and designed the simulations. F.N.B. and J.K. performed simulations. F.N.B. analyzed the data. All authors discussed the results, analyses, and interpretations. F.N.B. and J.K. wrote the paper with input from all authors. The authors declare no competing interests.

APPENDIX A: GENERALIZED LANGEVIN EQUATION WITH SPACE-INHOMOGENEOUS MEMORY FRICTION

1. Formulation of the GLE in a Markovian embedding

In the present section we show that the GLE with space-inhomogeneous memory, Eq. (1) from the main text, is equivalent to a $N + 1$ -dimensional dynamical system, in which the reaction coordinate $x(t)$ is coupled to N auxil-

iary degrees of freedom ($y_1(t), \dots, y_N(t)$), which we refer to as the heat bath. We assume that each of the y_i obeys an overdamped Langevin equation with random force $F_i(t)$ and friction magnitude γ_i . In analogy to the derivation by Zwanzig [3], we assume that the reaction coordinate is coupled to the heat bath via a nonlinear potential $U_{\text{hb}}(x, y_1, \dots, y_N) = \sum_{i=1}^N k_i [f_i(x) - y_i]^2 / 2$, where hb stands for heat bath, k_i determines the coupling strength between x and y_i , and the functions f_i will be used to obtain a space-inhomogeneous coupling between reaction coordinate and reservoir i . The total potential U_{tot} experienced by the dynamical system ($x(t), y_1(t), \dots, y_N(t)$) is then given as a sum

$$U_{\text{tot}}(x, y_1, \dots, y_N) = U(x) + U_{\text{hb}}(x, y_1, \dots, y_N), \quad (\text{A1})$$

where $U(x)$ is the double-well potential (5). The equations of motion for $x(t)$ and the $y_i(t)$ are then given by

$$m\ddot{x}(t) = - \sum_{i=1}^N k_i \{f_i[x(t)] - y_i(t)\} \partial_x f_i[x(t)] - (\partial_x U)[x(t)], \quad (\text{A2})$$

$$\gamma_i \dot{y}_i(t) = k_i \{f_i[x(t)] - y_i(t)\} + F_i(t). \quad (\text{A3})$$

The random forces F_i are Gaussian white noise with zero mean, $\langle F_i(t) \rangle = 0$, and covariances $\langle F_i(t) F_j(t') \rangle = 2\gamma_i k_B T \delta_{ij} \delta(t - t')$, so that the Langevin Eq. (A3) obeys the fluctuation-dissipation relation. To obtain a GLE for only the reaction coordinate $x(t)$, we eliminate the degrees of freedom $y_i(t)$ in Eq. (A2). For this, we use the formal solution of Eq. (A3), which is given by

$$y_i(t) = y_i(0) e^{-t/\tau_i} + \tau_i^{-1} \int_0^t dt' e^{-(t-t')/\tau_i} f_i[x(t')] + \int_0^t dt' e^{-(t-t')/\tau_i} \frac{F_i(t')}{\gamma_i} \quad (\text{A4})$$

$$= \{y_i(0) - f_i[x(0)]\} e^{-t/\tau_i} + f_i[x(t)] - \int_0^t dt' e^{-(t-t')/\tau_i} \partial_x f_i[x(t')] \dot{x}(t') + \int_0^t dt' e^{-(t-t')/\tau_i} \frac{F_i(t')}{\gamma_i}, \quad (\text{A5})$$

where we define the relaxation time of reservoir i as $\tau_i = \gamma_i / k_i$. Substituting the formal solution for $y_i(t)$ into Eq. (A2), we obtain

$$m\ddot{x}(t) = - \int_0^t \Gamma[t - t', x(t), x(t')] \dot{x}(t') dt' - \partial_x U[x(t)] + \eta[x(t), t] \quad (\text{A6})$$

with the space-inhomogeneous memory function

$$\Gamma[t - t', x(t), x(t')] = \sum_{i=1}^N \frac{\gamma_i}{\tau_i} \partial_x f_i[x(t)] e^{-(t-t')/\tau_i} \partial_x f_i[x(t')], \quad (\text{A7})$$

and the random force

$$\begin{aligned} \eta[x(t), t] = & - \sum_{i=1}^N \frac{\gamma_i}{\tau_i} \partial_x f_i[x(t)] e^{-t/\tau_i} \{f_i[x(0)] - y_i(0)\} \\ & + \sum_{i=1}^N \frac{1}{\tau_i} \int_0^t dt' \partial_x f_i[x(t')] e^{-(t-t')/\tau_i} F_i(t'). \end{aligned} \quad (\text{A8})$$

How the coupling of the reaction coordinate to reservoir i varies with $x(t)$ is determined by the function $f_i[x(t)]$. To obtain an on-off coupling depending on the value of $x(t)$, as used in Eqs. (2) and (3), we choose functions

$$f_i(x) = \begin{cases} x, & x \in X_i \\ \min(X_i), & x < \min(X_i) \\ \max(X_i), & x \geq \max(X_i) \end{cases}, \quad (\text{A9})$$

where X_i is a spatial domain, which we assume to be a single interval, within which $x(t)$ couples to reservoir i . With this definition, the spatial derivative of f_i is the coupling function,

$$(\partial_x f_i)(x) = \chi_i(x) := \begin{cases} 1, & x \in X_i \\ 0, & x \notin X_i \end{cases}, \quad (\text{A10})$$

so that Eqs. (A2) and (A3) couple $x(t)$ and $y_i(t)$ if and only if $x(t) \in X_i$, equivalent to a local memory kernel in that regime; cf. Eq. (A7). Note that, strictly speaking, the derivative $\partial_x f_i$ is not single-valued at the two points, $x = \min(X_i)$, $\max(X_i)$; since the probability that the reaction coordinate takes either one of these values is zero, this is not an issue.

To simulate the GLE (1), we always use the equivalent formulation in terms of a dimensionless version of the Markovian system of Eqs. (A2) and (A3), given in Appendix A 3.

2. Generalized fluctuation-dissipation relation

We now show that the memory kernel (A7) and the random force (A8) obey the generalized fluctuation-dissipation relation

$$\langle \eta[x(t), t] \eta[x(t'), t'] \rangle = k_B T \Gamma[x(t), x(t'), t - t']. \quad (\text{A11})$$

To compute the autocorrelation on the left-hand side of Eq. (A11) for all times t, t' , and not just for times larger than the longest initial relaxation time $\max_i \{\tau_i\}$ of the heat bath, we need to specify initial conditions $y_i(0)$ for the auxiliary variables, which appear in Eq. (A8). For this we assume that, for given $x(0)$, the $y_i(0)$ are distributed according to the Boltzmann distribution pertaining to the potential U_{hb} , so that $y_i(0) - f_i[x(0)]$ are given by a Gaussian distribution with zero mean and variance $\langle \{y_i(0) - f_i[x(0)]\}^2 \rangle = k_B T \tau_i / \gamma_i$. With this initial condition, the autocorrelation of the noise $\eta[x(t), t]$ follows as

$$\begin{aligned} \langle \eta[x(t), t] \eta[x(t'), t'] \rangle & = \sum_{i=1}^N \left(\frac{\gamma_i}{\tau_i} \right)^2 \chi_i[x(t)] \chi_i[x(t')] e^{-(t+t')/\tau_i} \langle [f_i[x(0)] - y_i(0)]^2 \rangle \\ & + \sum_{i=1}^N \frac{1}{\tau_i^2} \int_0^t dt'' \int_0^{t'} dt''' \chi_i[x(t'')] \chi_i[x(t''')] \\ & \times e^{-(t-t''+t'-t''')/\tau_i} \langle F_i(t'') F_i(t''') \rangle. \end{aligned}$$

$$\begin{aligned} & = \sum_{i=1}^N k_B T \frac{\gamma_i}{\tau_i} \chi_i[x(t)] \chi_i[x(t')] e^{-(t+t')/\tau_i} \\ & + \sum_{i=1}^N \frac{1}{\tau_i^2} \chi_i[x(t)] \chi_i[x(t')] e^{-(t+t')/\tau_i} \\ & \times \int_0^t dt'' \int_0^{t'} dt''' e^{(t''+t''')/\tau_i} 2\gamma_i k_B T \delta(t'' - t''') \\ & = \sum_{i=1}^N k_B T \frac{\gamma_i}{\tau_i} \chi_i[x(t)] \chi_i[x(t')] e^{-(t+t')/\tau_i} \\ & + \sum_{i=1}^N 2k_B T \frac{\gamma_i}{\tau_i^2} \chi_i[x(t)] \chi_i[x(t')] e^{-(t+t')/\tau_i} \\ & \times \int_0^{\min(t, t')} dt'' e^{2t''/\tau_i} \\ & = \sum_{i=1}^N k_B T \frac{\gamma_i}{\tau_i} \chi_i[x(t)] \chi_i[x(t')] e^{-|t-t'|/\tau_i}. \end{aligned} \quad (\text{A12})$$

By comparing the result (A12) with the memory kernel (A7), we observe that the generalized fluctuation-dissipation relation Eq. (A11) holds.

3. Dimensionless formulation of the GLE

In the present section, we give the dimensionless version of both the GLE (1), as well as the equivalent Markovian system Eqs. (A2) and (A3). This in particular makes explicit how many independent parameters the GLE model has.

Using the typical length scale L of the potential Eq. (5), and the thermal energy $k_B T \equiv \beta^{-1}$ as energy scale, we define the diffusive time, $\tau_D = \beta L^2 \gamma$, which is the typical time a freely diffusing particle with friction constant $\gamma = \sum_i \gamma_i$ needs to travel a distance L in a flat potential landscape. We furthermore define the inertial timescale $\tau_m = m/\gamma$, on which inertia is dissipated.

Using the scales L, τ_D, τ_m, β , we rewrite the coupled Langevin Eqs. (A2) and (A3) in dimensionless form as

$$\begin{aligned} \frac{\tau_m}{\tau_D} \ddot{\tilde{x}}(\tilde{t}) = & - \sum_{i=1}^N \frac{\gamma_i}{\gamma} \frac{\tau_D}{\tau_i} \{ \tilde{f}_i[\tilde{x}(\tilde{t})] - \tilde{y}_i(\tilde{t}) \} \partial_{\tilde{x}} \tilde{f}_i[\tilde{x}(\tilde{t})] \\ & - (\partial_{\tilde{x}} \tilde{U})[\tilde{x}(\tilde{t})], \end{aligned} \quad (\text{A13})$$

$$\dot{\tilde{y}}_i(\tilde{t}) = \frac{\tau_D}{\tau_i} \{ \tilde{f}_i[\tilde{x}(\tilde{t})] - \tilde{y}_i(\tilde{t}) \} + \sqrt{\frac{\gamma}{\gamma_i}} \tilde{F}_i(\tilde{t}), \quad (\text{A14})$$

where $\tilde{t} := t/\tau_D$, $\tilde{x}(\tilde{t}) := x(t\tau_D)/L$, $\dot{\tilde{x}}(\tilde{t}) = \tau_D \dot{x}(t)/L$, $\ddot{\tilde{x}}(\tilde{t}) = \tau_D^2 \ddot{x}(t)/L$ are dimensionless time, position, velocity and acceleration. $-(\partial_{\tilde{x}} \tilde{U})(\tilde{x})$ is the dimensionless deterministic force corresponding to the quartic potential (5) and given by

$$-(\partial_{\tilde{x}} \tilde{U})(\tilde{x}) = -4\tilde{U}_0(\tilde{x}^2 - 1)\tilde{x} \quad (\text{A15})$$

with dimensionless barrier height $\tilde{U}_0 := \beta U_0$.

The dimensionless coupling between reaction coordinate and heat bath is given by $\tilde{f}_i(\tilde{x}) := f_i(L\tilde{x})/L$, so that

$$\tilde{f}_i(\tilde{x}) = \begin{cases} \tilde{x}, & \tilde{x} \in \tilde{X}_i \\ \min(\tilde{X}_i), & \tilde{x} < \min(\tilde{X}_i) \\ \max(\tilde{X}_i), & \tilde{x} \geq \max(\tilde{X}_i) \end{cases}, \quad (\text{A16})$$

where $\tilde{X}_i = X_i/L$, so that

$$(\partial_{\tilde{x}} \tilde{f}_i)(\tilde{x}) = \tilde{\chi}_i(\tilde{x}) = \begin{cases} 1, & \tilde{x} \in \tilde{X}_i \\ 0, & \tilde{x} \notin \tilde{X}_i. \end{cases} \quad (\text{A17})$$

The dimensionless random forces $\tilde{F}_i(\tilde{t}) = L/(k_B T) \sqrt{\gamma/\gamma_i} F_i(t)$ are Gaussian white noise with zero mean, and covariances $\langle \tilde{F}_i(\tilde{t}) \tilde{F}_j(\tilde{t}') \rangle = 2\delta_{ij}\delta(\tilde{t} - \tilde{t}')$.

As in Appendix A 1, we formally solve Eq. (A14), and substitute the result into Eq. (A13), to obtain the dimensionless GLE

$$\frac{\tau_m}{\tau_D} \ddot{\tilde{x}}(\tilde{t}) = - \int_0^{\tilde{t}} \tilde{\Gamma}[\tilde{t} - \tilde{t}', \tilde{x}(\tilde{t}), \tilde{x}(\tilde{t} - \tilde{t}')] \dot{\tilde{x}}(\tilde{t}') d\tilde{t}' - (\partial_{\tilde{x}} \tilde{U})[\tilde{x}(\tilde{t}), \tilde{t}], \quad (\text{A18})$$

with the dimensionless space-inhomogeneous memory kernel

$$\begin{aligned} & \tilde{\Gamma}[\tilde{t} - \tilde{t}', \tilde{x}(\tilde{t}), \tilde{x}(\tilde{t}')] \\ &= \sum_{i=1}^N \frac{\gamma_i}{\gamma} \frac{\tau_D}{\tau_i} \tilde{\chi}_i[\tilde{x}(\tilde{t})] \tilde{\chi}_i[\tilde{x}(\tilde{t}')] \exp\left[-\frac{\tau_D}{\tau_i}(\tilde{t} - \tilde{t}')\right], \end{aligned} \quad (\text{A19})$$

and the dimensionless random force $\tilde{\eta}[\tilde{x}(\tilde{t}), \tilde{t}] := \beta\eta[x(t), t]/L$. Instead of explicitly eliminating the heat-bath variables, Eqs. (A18) and (A19), can also be obtained by directly recasting Eqs. (A6) and (A7), in dimensionless form. Similarly to Eq. (A11), the dimensionless memory kernel $\tilde{\Gamma}$ and random force $\tilde{\eta}$ obey the generalized fluctuation-dissipation theorem

$$\langle \tilde{\eta}[\tilde{x}(\tilde{t}), \tilde{t}] \tilde{\eta}[\tilde{x}(\tilde{t}'), \tilde{t}'] \rangle = \tilde{\Gamma}[\tilde{t} - \tilde{t}', \tilde{x}(\tilde{t}), \tilde{x}(\tilde{t}')]. \quad (\text{A20})$$

APPENDIX B: RATE THEORIES

1. Formulas for rate theories considered in the main text

In the present section we recall the formulas used to evaluate the various rate theories we consider in the main text.

a. Transition-state theory

While we do not explicitly show results from transition-state theory (TST) [58] in the main text, the TST escape rate appears in several of the rate theories we consider. According to TST, for a parabolic free-energy in the reactant state, the mean escape time is given as [58]

$$\tau_{\text{TST}} = \frac{2\pi}{\omega_{\min}} e^{\beta U_0}, \quad (\text{B1})$$

where as before U_0 denotes the barrier height, $\beta^{-1} = k_B T$ is the thermal energy, and the well frequency $\omega_{\min} = \sqrt{U''_{\min}/m}$ contains the curvature $U''_{\min} := U''(x_{\min})$ at the minimum x_{\min} of the potential well from which the particle escapes.

b. Kramers' theory

Kramers considered the escape from a potential well for a particle described by the Markovian inertial Langevin equation,

for both the limits of medium-to-high friction, and low friction [11]. For the medium-to-high friction regime he obtained

$$\tau_{\text{Kr}}^{\text{hf}} = \left[\left(\frac{\gamma^2}{4m^2} + \omega_{\max}^2 \right)^{1/2} - \frac{\gamma}{2m} \right]^{-1} \omega_{\max} \tau_{\text{TST}}, \quad (\text{B2})$$

while in the low-friction limit, he derived

$$\tau_{\text{Kr}}^{\text{lf}} = \frac{m}{\gamma \beta U_0} e^{\beta U_0}, \quad (\text{B3})$$

where the barrier frequency $\omega_{\max} = \sqrt{-U''_{\max}/m}$ contains the curvature $U''_{\max} := U''(x_{\max})$ at the barrier top x_{\max} . Note the opposite scaling of both equations with respect to the friction constant γ : While for medium-to-high friction it holds that $\tau_{\text{Kr}}^{\text{hf}} \sim \gamma$, for low friction we have $\tau_{\text{Kr}}^{\text{lf}} \sim \gamma^{-1}$.

c. Mel'nikov and Meshkov theory

Mel'nikov and Meshkov [15] (MM) derived a solution to the Kramers' problem which is valid for all values of the friction, and hence bridges the two asymptotic expressions Eqs. (B2) and (B3). The MM result is given by

$$\tau_{\text{MM}} = A^{-1}(\Delta) \left[\left(\frac{\gamma^2}{4m^2} + \omega_{\max}^2 \right)^{1/2} - \frac{\gamma}{2m} \right]^{-1} \omega_{\max} \tau_{\text{TST}}, \quad (\text{B4})$$

$$A(\Delta) = \exp \left[\frac{2}{\pi} \int_0^{\frac{\pi}{2}} \ln[1 - e^{-\Delta/[4\cos^2(x)]}] dx \right], \quad (\text{B5})$$

$$\Delta = 2\sqrt{2} \frac{\gamma}{\sqrt{m}} \beta \int_{-\sqrt{2}L}^0 \sqrt{U_0 - U(x)} dx. \quad (\text{B6})$$

d. Grote and Hynes theory

While both Kramers' and Mel'nikov and Meshkov theory consider Markovian dynamics, Grote and Hynes [13] developed a theory for the mean first-passage time, τ_{MFP} , under the influence of memory effects. Their expression for the case where the dynamics in the potential well relax fast, and only memory effects on the barrier are relevant, is given by

$$\tau_{\text{GH}} = \frac{\omega_{\max}}{\lambda} \tau_{\text{TST}}, \quad (\text{B7})$$

where $\tilde{\Gamma}(\lambda)$ denotes the Laplace-transformed memory friction kernel $\Gamma(t)$ at the barrier top, and the real reactive frequency $\lambda > 0$ is given as the solution of the equation

$$\lambda = \frac{\omega_{\max}^2}{\lambda + \tilde{\Gamma}(\lambda)/m}. \quad (\text{B8})$$

Thus, for a single exponential kernel $\Gamma(t) = \gamma e^{-t/\tau}/\tau$, λ is calculated from the cubic equation

$$\lambda^3 + \frac{\lambda^2}{\tau} + \left(\frac{\gamma}{m\tau} - \omega_{\max}^2 \right) \lambda = \frac{\omega_{\max}^2}{\tau}. \quad (\text{B9})$$

Note that, either in the inertial, $m \rightarrow \infty$, or in the long memory limit, $\tau \rightarrow \infty$, it follows that $\lambda = \omega_{\max}$ and the GH theory collapses onto the transition-state theory result, $\tau_{\text{GH}} = \tau_{\text{TST}}$ in Eq. (B7).

Furthermore, in the case of instantaneous, i.e., delta-correlated friction, $\Gamma(t) = 2\gamma\delta(t)$ and $\tilde{\Gamma}(\lambda) = \gamma$, it follows

$\lambda = (\gamma^2/(4m^2) + \omega_{\max}^2)^{1/2} - \gamma/(2m)$, which results in $\tau_{\text{GH}} = \tau_{\text{Kr}}^{\text{hf}}$, the Kramers high-friction result in Eq. (B2).

e. Heuristic formula

In our previous work we constructed a heuristic formula that agrees with both the theory by Pollak *et al.* [34] (PGH) and numerical simulations of τ_{MFP} in the double-well potential Eq. (5), and a GLE with a global single-exponential memory kernel with friction magnitude γ and memory time τ [21,35]. Using the diffusive and inertial timescales $\tau_D = \gamma\beta L^2$ and $\tau_m = m/\gamma$, the heuristic formula is given by

$$\frac{\tau_{\text{emp.}}}{\tau_D} = \frac{e^{\beta U_0}}{\beta U_0} \left[\frac{\pi}{2\sqrt{2}} \left(1 + 10\beta U_0 \frac{\tau}{\tau_D} \right)^{-1} + \frac{\tau_m}{\tau_D} + 2\sqrt{\beta U_0 \frac{\tau_m}{\tau_D}} + 4\beta U_0 \frac{\tau^2}{\tau_D^2} \right]. \quad (\text{B10})$$

2. Evaluation of rate theories for a space-inhomogeneous memory kernel

Whenever we evaluate a rate theory for the effective friction parameters of a region, we use the respective regional friction and memory parameters, or equivalently τ_i , $\tau_{D,i} = L^2\beta\gamma_i$, $\tau_{m,i} = m/\gamma_i$. On the other hand, in plots we always rescale the τ_{MFP} as well as the parameters using the diffusive- and inertial times $\tau_D = L^2\beta\gamma$, $\tau_m = m/\gamma$, which correspond to the total friction magnitude $\gamma = \sum_i \gamma_i$. In the present section we state the relevant relations between these local and global timescales.

The relation between the local and global diffusive and inertial timescales is given by

$$\tau_{D,i} = L^2\beta\gamma_i = \frac{\gamma_i}{\gamma} L^2\beta\gamma = \frac{\gamma_i}{\gamma} \tau_D, \quad (\text{B11})$$

$$\tau_{m,i} = \frac{m}{\gamma_i} = \frac{\gamma}{\gamma_i} \frac{m}{\gamma} = \frac{\gamma}{\gamma_i} \tau_m, \quad (\text{B12})$$

so that

$$\frac{\tau_{m,i}}{\tau_{D,i}} = \left(\frac{\gamma}{\gamma_i} \right)^2 \frac{\tau_m}{\tau_D}, \quad (\text{B13})$$

$$\frac{\tau_i}{\tau_{D,i}} = \frac{\gamma}{\gamma_i} \frac{\tau_i}{\tau_D}, \quad (\text{B14})$$

$$\frac{\tau_{\text{MFP}}}{\tau_{D,i}} = \frac{\gamma}{\gamma_i} \frac{\tau_{\text{MFP}}}{\tau_D}. \quad (\text{B15})$$

Therefore, if we want to calculate τ_{MFP}/τ_D for region i using a rate theory for globally homogeneous friction, we have to evaluate

$$\frac{\tau_{\text{MFP}}}{\tau_D} = \frac{\gamma_i}{\gamma} \frac{\tau_{\text{MFP}}}{\tau_{D,i}} \Bigg|_{(\gamma/\gamma_i)^2 \tau_m/\tau_D, (\gamma/\gamma_i)\tau_i/\tau_D}, \quad (\text{B16})$$

where the first argument $(\gamma/\gamma_i)^2 \tau_m/\tau_D$ is the argument for the dimensionless inertial timescale τ_m/τ_D in the rate theory, and the second argument $(\gamma/\gamma_i)\tau_i/\tau_D$ is the argument for the dimensionless single-exponential memory τ_Γ/τ_D in the rate theory.

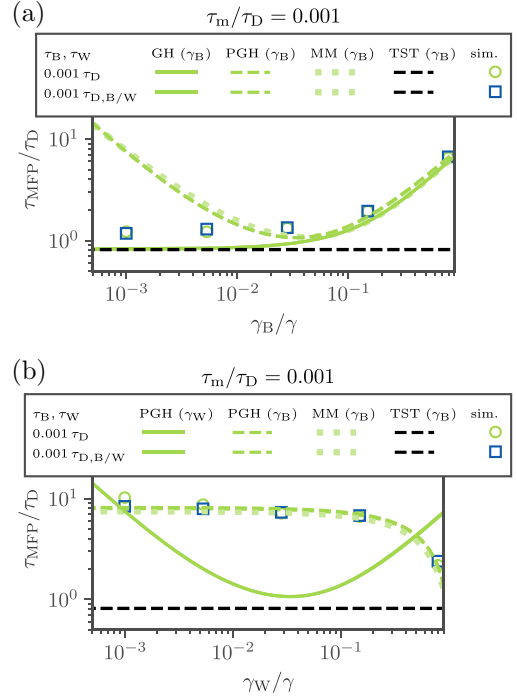


FIG. 4. MFPT, τ_{MFP}/τ_D , for various single-exponential barrier and well-memory friction parameters, compared with analytic predictions given by Grote and Hynes [13] [GH, solid line in (a)], Mel'nikov and Meshkov [15] (MM, dotted lines), Pollak *et al.* [34] (PGH, evaluated using the heuristic formula [21]), and transition-state theory (TST, black broken lines). The numerical data are shown for equal barrier and well-friction times, $\tau_B/\tau_D = \tau_W/\tau_D = 10^{-3}$, and the inertial timescale is fixed in the high-friction regime $\tau_m/\tau_D = 10^{-3}$. Dark blue square markers denote data for which the local friction timescales are kept constant, $\tau_B/\tau_{D,B} = \tau_W/\tau_{D,W} = 10^{-3}$, instead of the global ones. (a) Results for the limit $\gamma_B/\gamma \ll 1$, the limit of Markovian low friction on the barrier. (b) Results for the limit $\gamma_W/\gamma \ll 1$, the limit of Markovian low friction in the well.

APPENDIX C: FURTHER COMPARISONS OF NUMERICAL DATA WITH RATE THEORIES

1. Very unequal friction coefficients in well and barrier regions

In Fig. 2(d) above we show both the well- and barrier-evaluated MM predictions for high friction, $\tau_m/\tau_D = 10^{-4}$. Both curves show a nonmonotonic behavior as a function of the barrier friction magnitude γ_B/γ : Whereas the barrier-evaluated MM theory displays a minimum at small γ_B/γ , the well-evaluated MM prediction for τ_{MFP} becomes minimal at γ_B/γ close to 1. We here investigate these two limits in detail by performing simulations for both $\gamma_B/\gamma \ll 1$ and $1 - \gamma_B/\gamma = \gamma_W/\gamma \ll 1$. We show the results in Fig. 4, where we consider an inertial timescale of $\tau_m/\tau_D = 10^{-3}$ and equal friction timescales in the well and barrier, $\tau_B/\tau_D = \tau_W/\tau_D = 10^{-3}$.

In Fig. 4(a) we consider the limit $\gamma_B/\gamma \ll 1$, i.e., the limit of Markovian low friction on the barrier. While the MM and PGH theories, both evaluated for the barrier friction parameters, show a nonmonotonic trend (namely the Kramers turnover), the numerical τ_{MFP} (light green circles) levels off to

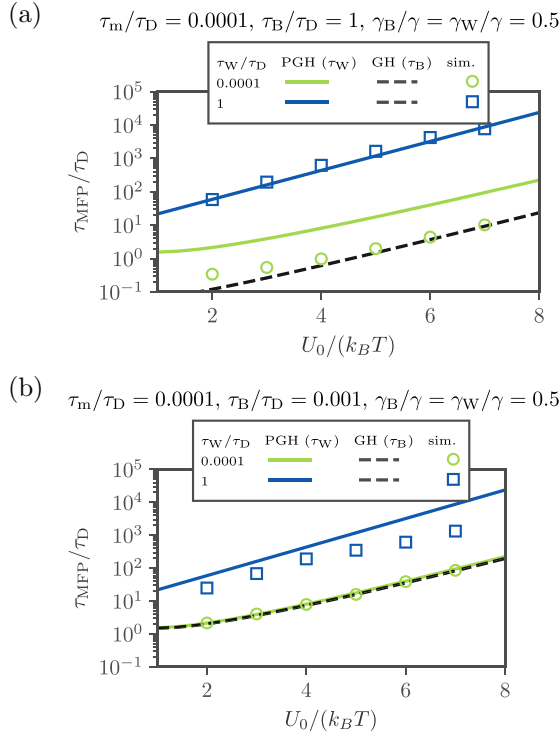


FIG. 5. MFPT, τ_{MFP}/τ_D , for various single-exponential barrier and well-friction parameters, shown as a function of the barrier height βU_0 . The numerical data are shown for two well-friction times, $\tau_W/\tau_D = 10^{-4}$ and $\tau_W/\tau_D = 1$, fixed barrier-friction time $\tau_B/\tau_D = 1$ (a) and $\tau_B/\tau_D = 10^{-3}$ (b), always for equal friction constants $\gamma_B/\gamma = \gamma_W/\gamma = 1/2$. The inertial timescale is fixed in the high-friction regime $\tau_m/\tau_D = 10^{-4}$. For comparison, predictions by Grote and Hynes [13] (GH, broken lines) and Pollak *et al.* [34] (PGH, solid lines, evaluated using the heuristic formula [21]) are also shown.

a constant for small γ_B/γ , with a value close to the prediction of transition-state theory (black broken line). This limit is also correctly recovered by the GH theory evaluated for the barrier friction parameters (light green solid line). Therefore, for $\gamma_B/\gamma \ll 1$, the GH theory outperforms MM theory and PGH theory. This is in contrast to the results shown in the main text in Figs. 2(a), 2(d), and 2(e), where the local friction magnitudes are considered to be within one order of magnitude, and the well-friction evaluated MM theory describes the numerical data correctly.

We discuss the opposite limit $\gamma_W/\gamma \ll 1$ in Fig. 4(b). Here the numerical τ_{MFP} (light green circles) is consistent with both the MM and PGH theories, evaluated using the barrier parameters, and markedly different from the predictions of transition-state theory and the PGH theory evaluated using the well parameters. The agreement of barrier-evaluated theories and the numerical data indicates that the system is described by the Kramers high-friction limit. At first sight this might seem surprising, because for $\gamma_W/\gamma \ll 1$ the local dynamics in the well is clearly underdamped, as for $\gamma_W/\gamma = 10^{-3}$ we have $\tau_{m,W}/\tau_{D,W} = 10^3$. However, since for $\gamma_W/\gamma \ll 1$ we have $\tau_{D,W} \ll \tau_{D,B}$, even though the mean time a particle in the well needs to reach the barrier is a large multiple of $\tau_{D,W}$, this time

may still be much smaller than the time to diffusively cross the barrier (which depends on $\tau_{D,B}$). Therefore, for $\gamma_W/\gamma \ll 1$, even though the well dynamics is in the energy diffusion limit, the crossing over the barrier can still be the rate-limiting step of the escape process.

Furthermore, we note that in both Figs. 4(a) and 4(b), for the lowest value of the local friction magnitude $\gamma_i/\gamma = 10^{-3}$, the local friction times, $\tau_i/\tau_{D,i} = 1$, are not anymore in the Markovian limit. To exclude local non-Markovian effects influencing the shown τ_{MFP} , we also show numerical data for constant local friction times, $\tau_B/\tau_{D,B} = \tau_W/\tau_{D,W} = 10^{-3}$ (dark blue squares) in Figs. 4(a) and 4(b). These data are almost identical to the data at constant τ_B/τ_D , τ_W/τ_D , so we conclude that non-Markovian effects remain negligible for the parameter regime shown.

2. Variation of barrier height

In the main text, we consider numerical results and rate theories for the barrier height $\beta U_0 = 3$. In Fig. 5 we compare numerical results for barrier heights ranging from $\beta U_0 = 2$ to $\beta U_0 = 7$ to rate-theory predictions, and find that conclusions drawn in the main text remain true also for larger barrier heights.

While in Fig. 5(a) we show results for non-Markovian barrier dynamics $\tau_B/\tau_D = 1$, in Fig. 5(b) we consider a barrier with Markovian dynamics, $\tau_B/\tau_D = 0.001$. For both subplots we use $\gamma_W/\gamma = \gamma_B/\gamma = 0.5$, i.e., an equal partitioning of the total friction magnitude to well and barrier, and high friction $\tau_m/\tau_D = 10^{-4}$. For both subplots, we consider two representative parameters for the well-friction time τ_W/τ_D . The results for $\tau_W/\tau_D = 10^{-4}$, shown as light green circles in Fig. 5, correspond to the Markovian high-well-friction regime, for which the dynamics are predicted by the GH theory. The dark blue squares in the figure correspond to τ_{MFP} for well-friction time $\tau_W/\tau_D = 1$, which corresponds to the long-well-memory regime where τ_{MFP} is predicted by the PGH theory, evaluated using the memory kernel parameters at the potential well. As Fig. 5(b) demonstrates, the “Markovian-barrier acceleration” regime discussed in detail in the main text also exists for larger barrier heights.

Overall, Fig. 5 shows that the predictions from the main text are consistent with the numerical data for all barrier heights $\beta U_0 \in [2, 7]$ considered here. In fact the predictions seem to improve for higher barriers. The exponential dependence of τ_{MFP} on the barrier-height, known since Arrhenius [59], is also well visible in our semilogarithmic representation of the data.

3. Variation of inertial timescale

In Fig. 3 we consider barrier crossing for the high-friction regime $\tau_m/\tau_D = 10^{-4}$, while the friction magnitudes are equal $\gamma_B/\gamma = \gamma_W/\gamma = 0.5$ and the friction memory times in the well τ_W/τ_D and on the barrier τ_B/τ_D are varied. In Fig. 6 we show additional numerical and analytical τ_{MFP} for larger inertial times. We consider the inertial times $\tau_m/\tau_D = 10^{-4}$ [Figs. 6(a)–6(c)], 10^{-2} [Figs. 6(d)–6(f)], and 1 [Figs. 6(g)–6(i)]. While the first column of Fig. 6 shows the rescaled τ_{MFP} as a function of the barrier-friction time τ_B/τ_D for various

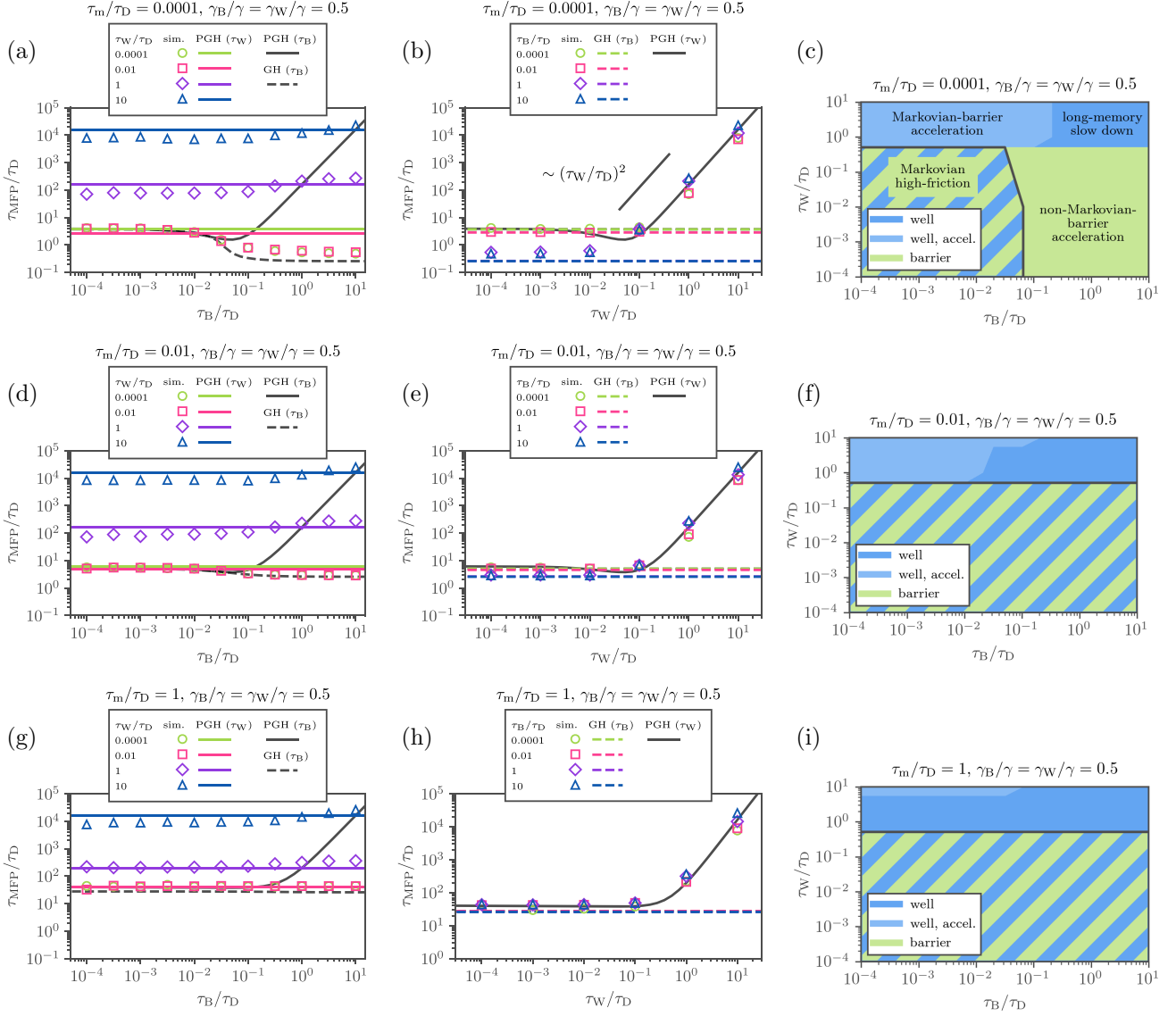


FIG. 6. MFPT, τ_{MFP}/τ_D , for different barrier memory friction, and well memory friction, obtained from numerical simulations (data points) and compared with analytic predictions given by Grote and Hynes [13] (GH, broken lines) and Pollak *et al.* [34] (PGH, solid lines, evaluated using the heuristic formula [21]). The data are shown for various barrier-friction τ_B/τ_D and well-friction times τ_W/τ_D and equal friction magnitudes $\gamma_B/\gamma = \gamma_W/\gamma = 0.5$. The inertial timescale is constant and different in each row (a–c: $\tau_m/\tau_D = 10^{-4}$, d–f: $\tau_m/\tau_D = 10^{-2}$, g–i: $\tau_m/\tau_D = 1$). (a, d, g) τ_{MFP} plotted over the barrier-friction time τ_B/τ_D . The theories are shown for the respective barrier-friction time in black and in the case of the PGH theory for the well-friction time as colored solid lines. (b, e, h) τ_{MFP} plotted over the well-friction time τ_W/τ_D . The theories are shown for the respective well-friction time in black and in the case of the GH theory for the barrier-friction time as colored broken lines. (c, f, i) Contour plots of agreement of the simulation results with the theoretical predictions. The color denotes whether the simulated $\tau_{\text{MFP}} \in [1/3 \tau_{\text{theo}}, 3 \tau_{\text{theo}}]$, where τ_{theo} is calculated using either the GH theory with the barrier-friction parameters or the PGH theory with the well-friction parameters. The hatching indicates that both theoretical predictions agree with the simulated data. The light blue area denotes the “Markovian-barrier acceleration” of the PGH prediction for which we define $\tau_{\text{theo,MBA}} = 0.2 \tau_{\text{theo,PGH}}$.

values of the well-friction time τ_W/τ_D , in the second column we vary the well-friction time for several constant values of the barrier-friction time. In both the first and second columns, the appropriate analytic predictions including memory effects are given either by the GH theory, which is evaluated for the effective barrier-friction parameters, determined by τ_B (broken lines) or by the PGH theory (solid lines), which is evaluated for the effective well-friction parameters, given by τ_W . The third column of Fig. 6 depicts phase diagrams that sum-

marize for which parameters (τ_B/τ_D , τ_W/τ_D) the numerical data agree with the predictions of the GH theory or PGH theory. Note that [Figs. 6(a)–6(c)] are replots of Figs. 3(a), 3(d), and 3(e).

Figure 6 shows that all conclusions drawn in the main text also hold true as τ_m/τ_D is varied, i.e., away from the high-friction limit. In particular, for larger inertial timescales τ_m/τ_D , the predictions for the τ_{MFP} are described globally by the PGH theory for the well-friction parameters.

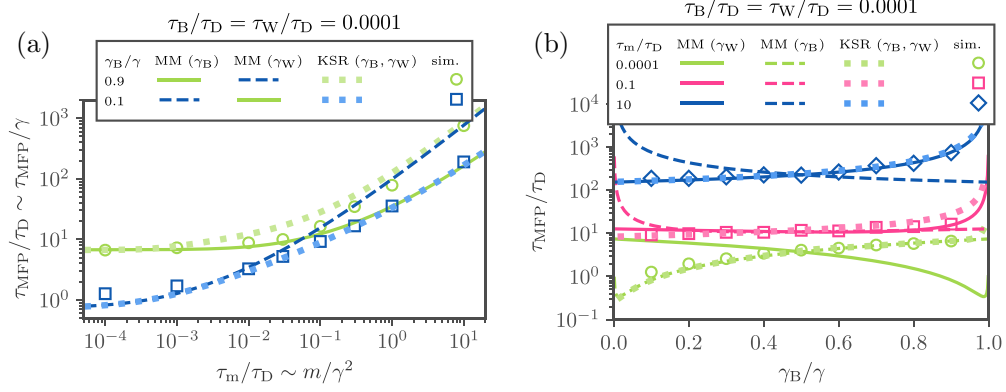


FIG. 7. MFPT, τ_{MFP}/τ_D , for different barrier memory friction, $\Gamma_B(t) = \gamma_B/\tau_B e^{-t/\tau_B}$ and well memory friction, $\Gamma_W(t) = \gamma_W/\tau_W e^{-t/\tau_W}$, obtained from numerical simulations (data points) and compared with analytic predictions given by Mel'nikov and Meshkov [15] (MM) as well as the predictions by Krishnan *et al.* [48] (KSR, dotted lines), equivalent to Figs. 2(a) and 2(d). The data are shown for equal memory times in the Markovian limit with $\tau_B/\tau_D = \tau_W/\tau_D = 10^{-4}$. (a) τ_{MFP} plotted over the inertial timescale τ_m/τ_D for different ratios of the barrier friction constant to total friction γ_B/γ . (b) τ_{MFP} plotted over γ_B/γ for various τ_m/τ_D . The predictions by MM are shown for the effective barrier-friction parameters, given by γ_B , as broken lines and for the effective well-friction parameters, given by γ_W , as solid lines.

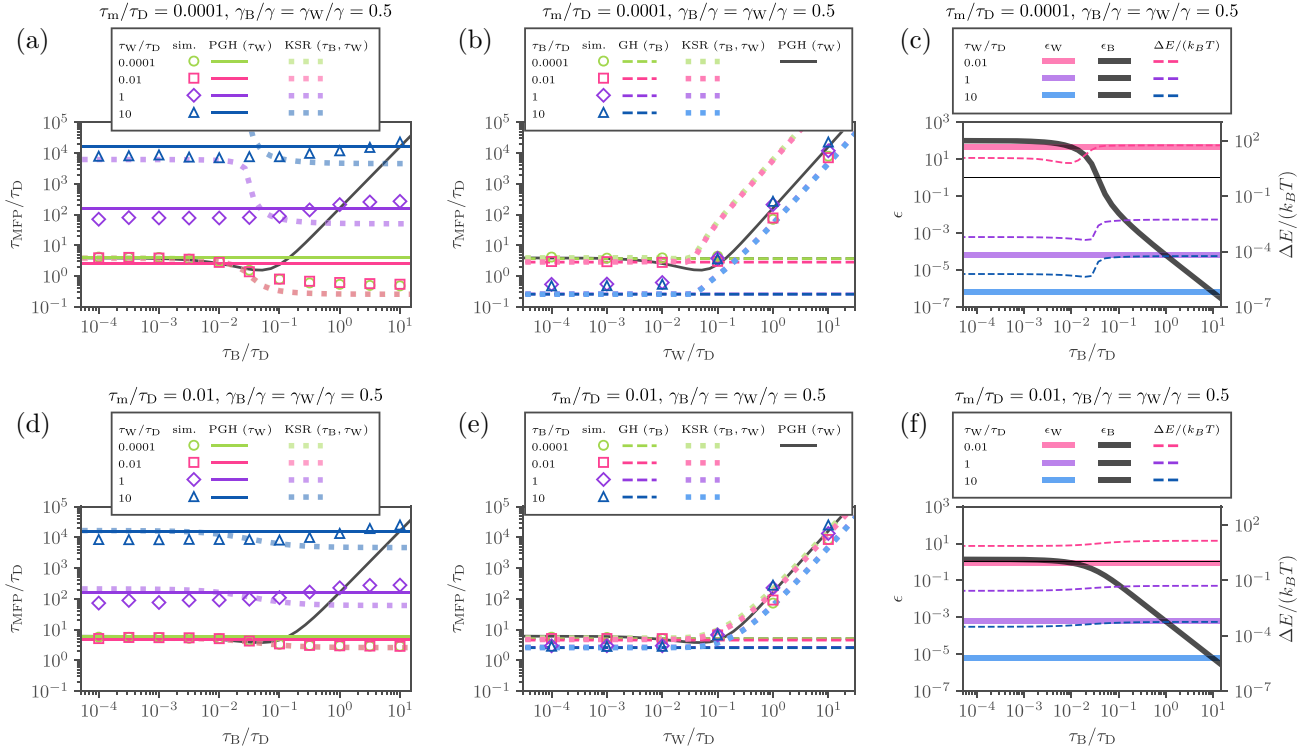


FIG. 8. MFPT, τ_{MFP}/τ_D , for different barrier memory friction and well memory friction, obtained from numerical simulations (data points) and compared with analytic predictions given by Grote and Hynes [13] (GH, broken lines) and by Pollak *et al.* [34] (PGH, solid lines, evaluated using the heuristic formula [21]), as well as predictions by Krishnan *et al.* [48] (KSR, dotted lines). The data are shown for various barrier-friction τ_B/τ_D and well-friction times τ_W/τ_D and equal friction constants $\gamma_B/\gamma = \gamma_W/\gamma = 1/2$. The inertial timescale is constant and different in each row (a–c: $\tau_m/\tau_D = 10^{-4}$, d–f: $\tau_m/\tau_D = 10^{-2}$). (a, d) τ_{MFP} plotted over the barrier-friction time τ_B/τ_D . The prediction by the PGH theory are shown for the respective barrier-friction time as black and for the well-friction time as colored solid lines. (b, e) τ_{MFP} plotted over the well-friction time τ_W/τ_D . The prediction by the PGH theory is shown for the respective well-friction time in black and in the case of GH theory for the barrier-friction time as colored broken lines. (c, f) Perturbation parameters ϵ_B for the barrier region and ϵ_W for the well region and energy loss $\Delta E/(k_B T)$, both relevant for stability of the KSR theory. The thin black horizontal line denotes the value 1.

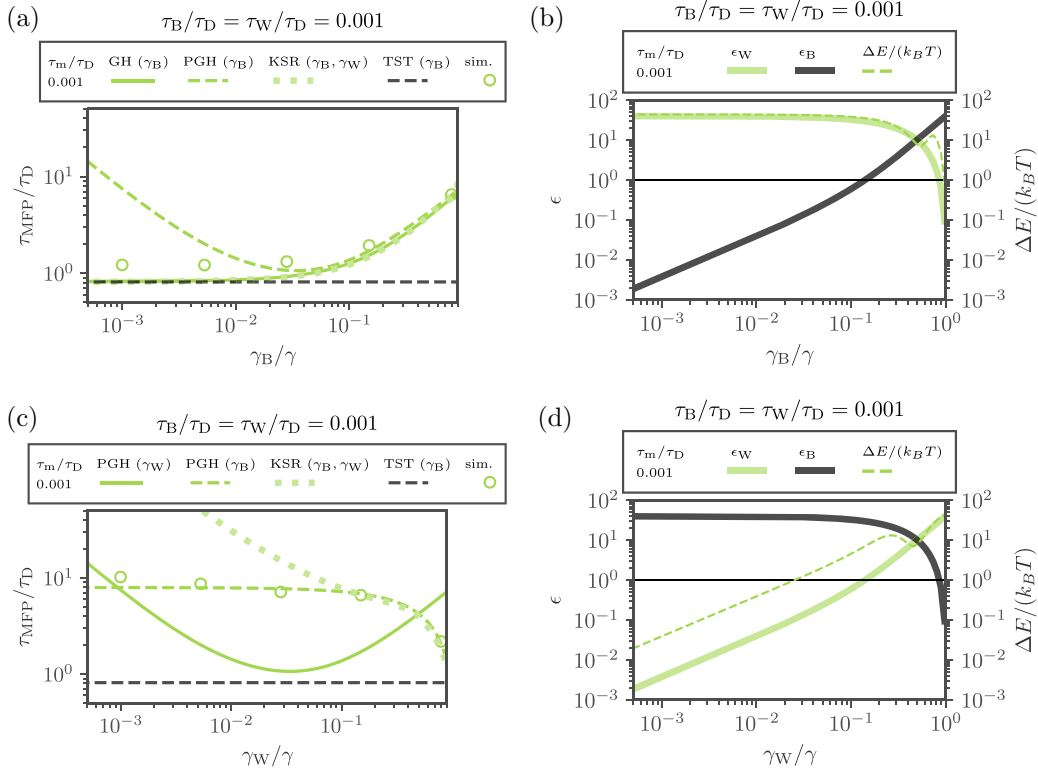


FIG. 9. MFPT, τ_{MFP}/τ_D , for various single-exponential barrier- and well-friction parameters, obtained from numerical simulations (data points) and compared with analytic predictions given by Grote and Hynes [13] [GH, solid line in (a)], Pollak *et al.* [34] (PGH, evaluated using the heuristic formula [21]), transition-state theory (TST, black broken lines), as well as the predictions by Krishnan *et al.* [48] (KSR, dotted lines). The numerical data are shown for equal barrier and well-friction times, $\tau_B/\tau_D = \tau_W/\tau_D = 10^{-3}$ and the inertial timescale is fixed in the high-friction regime $\tau_m/\tau_D = 10^{-3}$. (a) Results for the limit $\gamma_B/\gamma \ll 1$, the limit of Markovian low friction on the barrier. (c) Results for the limit $\gamma_W/\gamma \ll 1$, the limit of Markovian low friction in the well. (b, d) Perturbation parameters ϵ_B for the barrier region and ϵ_W for the well region and energy loss $\Delta E/(k_B T)$, both relevant for stability of the KSR theory. The thin black horizontal line denotes the value 1.

Furthermore, Figs. 6(d) and 6(g) show that the “Markovian-barrier acceleration” regime is also present for larger inertial times. On the other hand, the “non-Markovian-barrier acceleration” predicted by the GH theory vanishes.

4. Comparison of numerical results to KSR theory

In the present section, we compare our numerical τ_{MFP} with the predictions of a theory for barrier crossing with space-inhomogeneous memory friction. Krishnan, Singh, and Robinson (KSR) [48] derived an analytic theory for τ_{MFP} in a piecewise harmonic potential with different well and barrier memory friction; this theory is based on the formalism by Pollak, Grabert, and Hänggi [34]. The analytical KSR predictions for τ_{MFP} had not been compared to numerical simulations in the literature.

The KSR model takes as input the memory-friction kernels for the well and barrier regions, for both of which we consider single exponentials, the particle mass $m = \tau_m \gamma$, the local angular frequencies of the potential for the well, $\omega_0 = (\partial_x^2 U)(x = -L)/m$ and barrier $\omega_b = -(\partial_x^2 U)(x = 0)/m$, and the barrier height $\beta U_0 = 3$, where as before $U(x)$ is the quartic potential (5).

We now compare the predictions of KSR theory with the same numerical data as considered in Figs. 2 and 3.

First, in Fig. 7 we consider the data from Fig. 2. For a detailed discussion of the data we refer to the main text, as this section focuses on evaluating the quality of the KSR theory with respect to the other theories. For the Markovian limit, i.e., $\tau_W/\tau_D = \tau_B/\tau_D \ll 1$, we generally observe good agreement between numerical data and KSR theory throughout Fig. 7. However, the predictions by MM using effective local parameters perform slightly better in the whole parameter range. Of course, the true strength of the model by KSR here is the correct interpolation between barrier- and well-dominated dynamics, which needs to be chosen by hand in the evaluation of MM theory. This is most clearly seen in Fig. 2, where KSR theory switches between the barrier-dominated and well-dominated MM predictions as τ_m/τ_D is increased.

The data of Fig. 3(a) and 3(d) are discussed in this section in Figs. 8(a) and 8(b), where $\tau_m/\tau_D = 10^{-4}$. While the predictions by KSR again interpolate correctly between well- and barrier-dominated dynamics, in the regime where $\tau_W/\tau_D \geq 0.1$ and $\tau_B/\tau_D \leq 0.1$, we observe significant deviations between the numerical τ_{MFP} and the corresponding KSR prediction. As can be seen clearly in the upper left corner of Fig. 3(a) and the right side of Fig. 3(b), the numerical and analytical data can deviate by several orders of magnitude. For larger inertial timescales, these deviations become smaller as shown in Figs. 8(c) and 8(d) where $\tau_m/\tau_D = 10^{-2}$. We

note that KSR throughout predicts a barrier crossing speedup as τ_B/τ_D is increased [see Figs. 8(a) and 8(d)], whereas the numerical data display the “Markovian-barrier acceleration” behavior for $\tau_W/\tau_D \gtrsim 1$, for which barrier crossing is in fact slower as τ_B/τ_D is increased. Possible explanations for the deviations observed in Figs. 7 and 8 are discussed in the following.

To rationalize the deviations between numerical and analytical predictions, we point out that KSR themselves state that their theory is not to be expected to be reliable if $\epsilon_B \gtrsim 1$ in the barrier region or $\epsilon_W \gtrsim 1$ in the well region (note that ϵ and ϵ' are used in the original work [48]). The perturbation parameters ϵ_B , ϵ_W represent a measure for the strength of coupling between reaction coordinate and heat bath, and are defined as $\epsilon_B = \gamma_B/[2m\lambda_B(1 + \tau_B\lambda_B)^2]$ and $\epsilon_W = \gamma_W/[2m\lambda_W(1 + \tau_W\lambda_W)^2]$, with λ_B and λ_W the GH frequencies which solve Eq. (B8) for the respective memory kernels (well or barrier). These conditions are easily violated in the case of small inertial timescales $\tau_m = m/\gamma$, as Fig. 8(c) shows. However, a similar perturbation parameter ϵ is also relevant for the applicability of the PGH theory, and those authors note in their paper that the PGH theory remains valid even for large ϵ , if at the same time the energy loss per cycle through the well region is large, $\beta\Delta E > 1$ [34]. More so, the PGH predictions have been shown to globally agree well with numerical results obtained from a homogeneous memory kernel [35].

The clear deviations between KSR theory and the numerical results in Fig. 8(a), observed for small τ_B/τ_D and large τ_W/τ_D (dark purple and dark blue lines), can be rationalized by the simultaneous breakdown of both the conditions on the pair ϵ_B , ϵ_W , and $\beta\Delta E$: as Fig. 8(c) shows, in the regime where deviations between theory and numerical data are observed, $\epsilon_B \gtrsim 1$ while $\beta\Delta E \ll 1$. In contrast to that, Fig. 8(f) shows the perturbation parameters and energy loss per cycle for

slightly larger inertial times $\tau_m/\tau_D = 0.01$. Here the conditions $\epsilon_B < 1$ and $\epsilon_W < 1$ are met and the predictions agree with the simulation data in Figs. 8(c) and 8(e).

In Fig. 4 we consider τ_{MFP} for the cases where $\gamma_B/\gamma \ll 1$ and $\gamma_W/\gamma \ll 1$, i.e., the scenario where the well- and barrier-friction magnitudes are very different. In Figs. 9(a) and 9(c) we compare the numerical results for τ_{MFP} with KSR theory. As can be observed in Fig. 9(a), KSR theory (light green dotted line) correctly captures the limit $\gamma_B/\gamma \ll 1$, i.e., the limit of Markovian low friction on the barrier. However, Fig. 9(c) shows that KSR theory does not capture the opposite limit. For $\gamma_W/\gamma \ll 1$, KSR theory predicts a significant slow-down, which is not confirmed by simulation data. The breakdown of KSR theory is again understood by considering the perturbation parameters ϵ_B , ϵ_W and the energy loss $\Delta E/(k_B T)$, which are plotted in Figs. 9(b) and 9(d) for the respective data. As previously discussed for the data in Fig. 8, KSR theory breaks down whenever the energy loss per cycle in the well region is small, $\Delta E/(k_B T) \ll 1$, while the coupling to the barrier heat bath is strong, $\epsilon_B \gtrsim 1$. This is again the case for the data in Fig. 9(c), as can be seen from the corresponding perturbation parameters in Fig. 9(d).

In summary, while KSR theory does capture the crossover from well-dominated to barrier-dominated τ_{MFP} , the theory captures neither the “Markovian-barrier acceleration” regime, nor the limit $\gamma_W/\gamma \ll 1$. This can be explained by the assumptions underlying the KSR derivation, which are not fulfilled in these regimes: In both regimes, the energy exchange with the well heat bath is weak (small $\beta\Delta E \ll 1$), while simultaneously the coupling to the barrier heat bath is strong ($\epsilon_B \gtrsim 1$). While in the “Markovian-barrier acceleration” regime, the weak energy exchange in the well is due to long memory, in the regime $\gamma_W/\gamma \ll 1$, the weak energy exchange is because of the small well friction.

-
- [1] R. Zwanzig, Memory effects in irreversible thermodynamics, *Phys. Rev.* **124**, 983 (1961).
- [2] H. Mori, Transport, collective motion, and Brownian motion, *Prog. Theor. Phys.* **33**, 423 (1965).
- [3] R. Zwanzig, Nonlinear generalized Langevin equations, *J. Stat. Phys.* **9**, 215 (1973).
- [4] R. Zwanzig, *Nonequilibrium Statistical Mechanics* (Oxford University Press, Oxford, 2001)
- [5] A. Berezhkovskii and A. Szabo, One-dimensional reaction coordinates for diffusive activated rate processes in many dimensions, *J. Chem. Phys.* **122**, 014503 (2005).
- [6] O. F. Lange and H. Grubmüller, Collective Langevin dynamics of conformational motions in proteins, *J. Chem. Phys.* **124**, 214903 (2006).
- [7] J. O. Daldrop, J. Kappler, F. N. Brünic, and R. R. Netz, Butane dihedral angle dynamics in water is dominated by internal friction, *Proc. Natl. Acad. Sci. USA* **115**, 5169 (2018).
- [8] J. Kappler, F. Noé, and R. R. Netz, Cyclization and Relaxation Dynamics of Finite-Length Collapsed Self-Avoiding Polymers, *Phys. Rev. Lett.* **122**, 067801 (2019).
- [9] R. Satija and D. E. Makarov, Generalized Langevin equation as a model for barrier crossing dynamics in biomolecular folding, *J. Phys. Chem. B* **123**, 802 (2019).
- [10] B. Lickert and G. Stock, Modeling non-Markovian data using Markov state and Langevin models, *J. Chem. Phys.* **153**, 244112 (2020).
- [11] H. Kramers, Brownian motion in a field of force and the diffusion model of chemical reactions, *Physica* **7**, 284 (1940).
- [12] D. Chandler, Statistical mechanics of isomerization dynamics in liquids and the transition state approximation, *J. Chem. Phys.* **68**, 2959 (1978).
- [13] R. F. Grote and J. T. Hynes, The stable states picture of chemical reactions. II. Rate constants for condensed and gas phase reaction models, *J. Chem. Phys.* **73**, 2715 (1980).
- [14] D. Chandler, Roles of classical dynamics and quantum dynamics on activated processes occurring in liquids, *J. Stat. Phys.* **42**, 49 (1986).

- [15] V. I. Mel'nikov and S. V. Meshkov, Theory of activated rate processes: Exact solution of the Kramers problem, *J. Chem. Phys.* **85**, 1018 (1986).
- [16] P. Hänggi, P. Talkner, and M. Borkovec, Reaction-rate theory: Fifty years after Kramers, *Rev. Mod. Phys.* **62**, 251 (1990).
- [17] V. I. Mel'nikov, The Kramers problem: Fifty years of development, *Phys. Rep.* **209**, 1 (1991).
- [18] R. B. Best and G. Hummer, Diffusive Model of Protein Folding Dynamics with Kramers Turnover in Rate, *Phys. Rev. Lett.* **96**, 228104 (2006).
- [19] G. Wilemski and M. Fixman, Diffusion-controlled intrachain reactions of polymers. II. Results for a pair of terminal reactive groups, *J. Chem. Phys.* **60**, 878 (1974).
- [20] A. Szabo, K. Schulten, and Z. Schulten, First passage time approach to diffusion controlled reactions, *J. Chem. Phys.* **72**, 4350 (1980).
- [21] J. Kappler, V. B. Hinrichsen, and R. R. Netz, Non-Markovian barrier crossing with two-time-scale memory is dominated by the faster memory component, *Eur. Phys. J. E* **42**, 119 (2019).
- [22] C. Ayaz, L. Tepper, F. N. Brünig, J. Kappler, J. O. Daldrop, and R. R. Netz, Non-Markovian modeling of protein folding, *Proc. Natl. Acad. Sci. USA* **118**, e2023856118 (2021).
- [23] J. E. Straub, M. Borkovec, and B. J. Berne, Calculation of dynamic friction on intramolecular degrees of freedom, *J. Phys. Chem.* **91**, 4995 (1987).
- [24] G. Ciccotti, M. Ferrario, J. T. Hynes, and R. Kapral, Dynamics of ion pair interconversion in a polar solvent, *J. Chem. Phys.* **93**, 7137 (1990).
- [25] I. Benjamin, L. L. Lee, Y. S. Li, A. Liu, and K. R. Wilson, Generalized Langevin model for molecular dynamics of an activated reaction in solution, *Chem. Phys.* **152**, 1 (1991).
- [26] R. Rey, E. Guàrdia, and J. A. Padró, Generalized Langevin dynamics simulation of activated processes in solution: Ion pair interconversion in water, *J. Chem. Phys.* **97**, 8276 (1992).
- [27] H. V. R. Annapureddy and L. X. Dang, Understanding the rates and molecular mechanism of water-exchange around aqueous ions using molecular simulations, *J. Phys. Chem. B* **118**, 8917 (2014).
- [28] H. Meyer, S. Wolf, G. Stock, and T. Schilling, A numerical procedure to evaluate memory effects in non-equilibrium coarse-grained models, *Adv. Theory Sim.* **4**, 2000197 (2021).
- [29] M. Tuckerman and B. J. Berne, Vibrational relaxation in simple fluids: Comparison of theory and simulation, *J. Chem. Phys.* **98**, 7301 (1993).
- [30] F. N. Brünig, O. Geburtig, A. von Canal, J. Kappler, and R. R. Netz, Time-dependent friction effects on vibrational infrared frequencies and line shapes of liquid water, *J. Phys. Chem. B* **126**, 1579 (2022).
- [31] R. Zwanzig, Ensemble method in the theory of irreversibility, *J. Chem. Phys.* **33**, 1338 (1960).
- [32] J. O. Daldrop, B. G. Kowalik, and R. R. Netz, External Potential Modifies Friction of Molecular Solutes in Water, *Phys. Rev. X* **7**, 041065 (2017).
- [33] B. Müller, J. Berner, C. Bechinger, and M. Krüger, Properties of a nonlinear bath: Experiments, theory, and a stochastic Prandtl-Tomlinson model, *New J. Phys.* **22**, 023014 (2020).
- [34] E. Pollak, H. Grabert, and P. Hänggi, Theory of activated rate processes for arbitrary frequency dependent friction: Solution of the turnover problem, *J. Chem. Phys.* **91**, 4073 (1989).
- [35] J. Kappler, J. O. Daldrop, F. N. Brünig, M. D. Boehle, and R. R. Netz, Memory-induced acceleration and slowdown of barrier crossing, *J. Chem. Phys.* **148**, 014903 (2018).
- [36] P. Talkner and H.-B. Braun, Transition rates of a non-Markovian Brownian particle in a double well potential, *J. Chem. Phys.* **88**, 7537 (1988).
- [37] J. E. Straub, M. Borkovec, and B. J. Berne, Non-Markovian activated rate processes: Comparison of current theories with numerical simulation data, *J. Chem. Phys.* **84**, 1788 (1986).
- [38] S. C. Tucker, M. E. Tuckerman, B. J. Berne, and E. Pollak, Comparison of rate theories for generalized Langevin dynamics, *J. Chem. Phys.* **95**, 5809 (1991).
- [39] R. Ianculescu and E. Pollak, A study of Kramers' turnover theory in the presence of exponential memory friction, *J. Chem. Phys.* **143**, 104104 (2015).
- [40] L. Lavacchi, J. Kappler, and R. R. Netz, Barrier crossing in the presence of multi-exponential memory functions with unequal friction amplitudes and memory times, *Europhys. Lett.* **131**, 40004 (2020).
- [41] A. Berezhkovskii and A. Szabo, Time scale separation leads to position-dependent diffusion along a slow coordinate, *J. Chem. Phys.* **135**, 074108 (2011).
- [42] G. Hummer, From transition paths to transition states and rate coefficients, *J. Chem. Phys.* **120**, 516 (2004).
- [43] M. Hinczewski, Y. von Hansen, J. Dzubiella, and R. R. Netz, How the diffusivity profile reduces the arbitrariness of protein folding free energies, *J. Chem. Phys.* **132**, 245103 (2010).
- [44] J. B. Straus, J. M. Gomez Llorente, and G. A. Voth, Manifestations of spatially dependent friction in classical activated rate processes, *J. Chem. Phys.* **98**, 4082 (1993).
- [45] E. Pollak and A. M. Berezhkovskii, Fokker-Planck equation for nonlinear stochastic dynamics in the presence of space and time dependent friction, *J. Chem. Phys.* **99**, 1344 (1993).
- [46] G. R. Haynes, G. A. Voth, and E. Pollak, A theory for the activated barrier crossing rate constant in systems influenced by space and time dependent friction, *J. Chem. Phys.* **101**, 7811 (1994).
- [47] S. Singh, R. Krishnan, and G. W. Robinson, Theory of activated rate processes with space-dependent friction, *Chem. Phys. Lett.* **175**, 338 (1990).
- [48] R. Krishnan, S. Singh, and G. W. Robinson, Space-dependent friction in the theory of activated rate processes: The Hamiltonian approach, *J. Chem. Phys.* **97**, 5516 (1992).
- [49] S. Singh and G. W. Robinson, Scaling in a model of chemical reaction rates with space-dependent friction, *J. Phys. Chem.* **98**, 7300 (1994).
- [50] J. O. Daldrop, W. K. Kim, and R. R. Netz, Transition paths are hot, *Europhys. Lett.* **113**, 18004 (2016).
- [51] A. F. Voter and J. D. Doll, Dynamical corrections to transition state theory for multistate systems: Surface self-diffusion in the rare-event regime, *J. Chem. Phys.* **82**, 80 (1985).
- [52] C. Ayaz, L. Scalfi, B. A. Dalton, and R. R. Netz, Generalized Langevin equation with a nonlinear potential of mean force and nonlinear memory friction from a hybrid projection scheme, *Phys. Rev. E* **105**, 054138 (2022).

- [53] H. Vroylandt, L. Goudenège, P. Monmarché, F. Pietrucci, and B. Rotenberg, Likelihood-based non-Markovian models from molecular dynamics, *Proc. Natl. Acad. Sci. USA* **119**, e2117586119 (2022).
- [54] S. A. M. Loos and S. H. L. Klapp, Irreversibility, heat and information flows induced by non-reciprocal interactions, *New J. Phys.* **22**, 123051 (2020).
- [55] S. Nakajima, On quantum theory of transport phenomena: Steady diffusion, *Prog. Theor. Phys.* **20**, 948 (1958).
- [56] G. W. Ford, J. T. Lewis, and R. F. O'Connell, Quantum Langevin equation, *Phys. Rev. A* **37**, 4419 (1988).
- [57] B. Carmeli and D. Chandler, Effective adiabatic approximation for a two level system coupled to a bath, *J. Chem. Phys.* **82**, 3400 (1985).
- [58] H. Eyring, The activated complex in chemical reactions, *J. Chem. Phys.* **3**, 107 (1935).
- [59] S. Arrhenius, Über die Reaktionsgeschwindigkeit bei der Inversion von Rohrzucker durch Säuren, *Z. Phys. Chem.* **4**, 226 (1889).